



ISSN: 0975-833X

Available online at <http://www.journalcra.com>

INTERNATIONAL JOURNAL
OF CURRENT RESEARCH

International Journal of Current Research
Vol. 11, Issue, 08, pp.6398-6428, August, 2019

DOI: <https://doi.org/10.24941/ijcr.36259.08.2019>

RESEARCH ARTICLE

SYNTHESIS, CHARACTERIZATION AND DFT CALCULATIONS OF SOME ARYL 1-(2,4-DINITRONAPHTHYL) ETHERS AND AMINES

^{2,*}Nagwa M. M. Hamada, ²Yasmen M. Moghazy, ¹Magda F. Fathalla, ³Yasser R. Elmarassi and ¹Ezzat A. Hamed

¹Chemistry Department, Faculty of Science, Alexandria University, P.O. 426 Ibrahimia, Alexandria 21321, Egypt

²Chemistry Department, Faculty of Education, Alexandria University, Alexandria 21526, Egypt

³Basic Science Department-Imam Abdulrahman Bin Faisal University (Dammam University), P. O. Box 2114 Dammam 31451, Kingdom of Saudi Arabia

ARTICLE INFO

Article History:

Received 11th May, 2019

Received in revised form

15th June, 2019

Accepted 13th July, 2019

Published online 31st August, 2019

Key Word:

Density Functional Theory,
Nucleophilic Attack,
Naphthyl Ethers, ¹HNMR.

*Corresponding author:

Nagwa M. M. Hamada

Copyright © 2019, Nagwa M. M. Hamada et al. This is an open access article distributed under the Creative Commons Attribution License, which permits unrestricted use, distribution, and reproduction in any medium, provided the original work is properly cited.

Citation: Nagwa M. M. Hamada, Yasmen M. Moghazy, Magda F. Fathalla, Yasser R. Elmarassi and Ezzat A. Hamed, 2019. "Synthesis, Characterization and DFT calculations of some aryl 1-(2,4-dinitronaphthyl) ethers and amines", *International Journal of Current Research*, 11, (08), 6398-6428.

ABSTRACT

The density functional theory (DFT) with B3LYP/6-311G (d, p) basis set is used for determination of chemical reactivity (stability) and selective sites of aryl 1-(2,4-dinitronaphthyl) ether and amine derivatives. The calculation of dihedral angles indicates that the phenyl and naphthyl rings are not planar. In addition, the molecular electrostatic potential maps and frontier molecular orbitals were performed at B3LYP/6-311G (d, p) level of theory. Mulliken, NBO atomic charge of both ethers and amines, IR, UV and ¹H NMR are calculated. DFT global chemical reactivity descriptors (chemical hardness, energy, electronic chemical potential and electrophilicity) are calculated for the title molecules and used to predict their relative stability and reactivity. The active sites for nucleophilic and electrophilic attacks have been chosen by relating them to the Fukui function. The regioselectivity of nucleophilic attack on ether is presumably achieved from calculating and comparing the energies of the activated complexes obtained from nucleophilic attack on C₁ and C₁'.

INTRODUCTION

Naphthalene and its derivatives are biologically (1) pharmaceutically (2) and industrially useful compounds. Particularly, naphthalene was studied because of its technological applications in a vast amount of industrial process. (3) In fact, naphthalene and its derivatives were used as a precursor for the synthesis of plastics and dyes, gamma-ray detector in photomultiplier tubes and also used in dye stuffs, synthetic resins, coatings, tanning agent, celluloid (4), pesticide (5) and insecticide (6). Several naphthalene is widely recognized that their metabolites are among the most toxic, carcinogenic, mutagenic atmospheric contaminants and in stimulating the release and deficiency of growth (7). N-phenyl-1-naphthylamine (PANA) are used in rubber and lubricating oils as well as antioxidants. (8) Studies have shown acute exposure to PANA may result in skin and kidney irritation, fatty degeneration of the liver, and diarrhea. Dermal exposures have resulted in pneumonia, lung abscesses and fatty degeneration of the liver. (9) PANA is also a potential carcinogen (10). N-phenyl-2-naphthylamine acts intracellularly as

a reactive compound in cell membranes producing irreversible, thus cumulative, damage over time in algae (11) and has been specific phytotoxic properties. The introduction of hydroxy-, nitro-, and methyl-substituents show clear excess toxicity as compared to baseline toxic effects. Recently, computational methods based on density functional theory (DFT) predict relatively accurate molecular structure with moderate computational effort (12). We successfully attempted to prepare new naphthyl ethers namely aryl 1-(2,4-dinitronaphthyl) ethers 1a-h and the corresponding amine products 2a-g and 3 resulting from their reactions with aniline derivatives 2a-g and piperidine 3, shown in Figure 1, as well as examine their antimicrobial activities. The aim is extended to study the regioselectivity between ipso naphthyl center and ipso aryl center in ethers towards aminonucleophiles. The optimized molecular structure of aryl 1-(2,4-dinitronaphthyl) ethers 1a-h is a step to know the reactivity of these ethers towards nucleophiles.

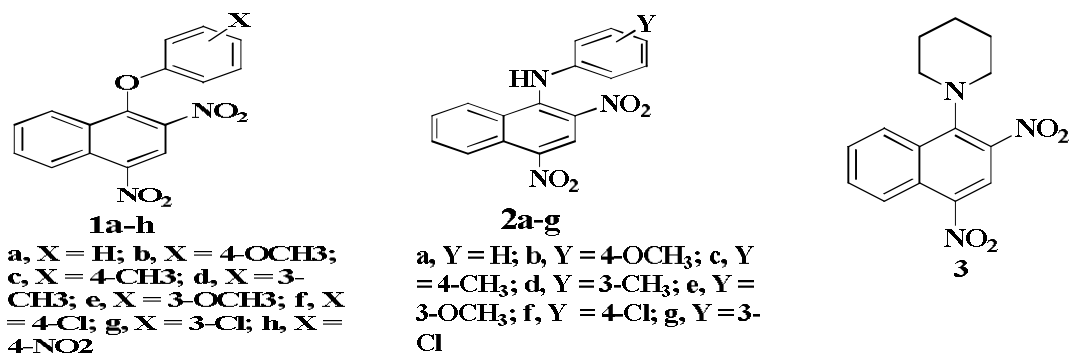
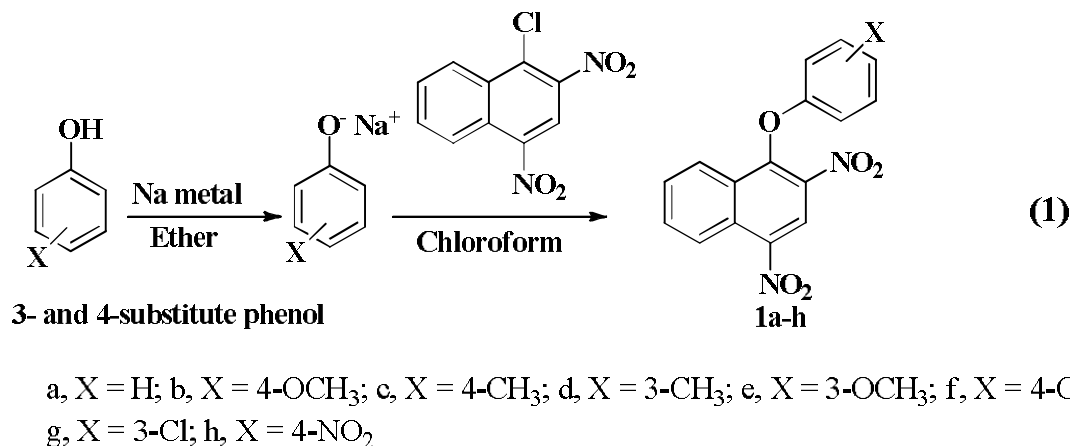


Figure 1. Structure of 1a-h, 2a-g and 3

RESULTS AND DISCUSSION

Synthesis and assignments of aryl ether 2,4-dinitronaphthyl 1a-h: 1-Aryl 1-(2,4-dinitronaphthyl) ethers 1a-h were prepared by substitution reaction of the chlorine atom of 1-chloro-2,4-dinitronaphthalene 5 with substituted phenoxide ions 4a-h, Equation (1). As expected, yields were found to be highly dependent on the nature of the *meta* and *para*-substituents in phenol; electron withdrawing substituents and electron donating substituents resulted in decreased and increased yield respectively. The chemical structures of compounds 1a-h are assigned from their UV, IR, ¹H NMR and elemental analysis.



Optimized Molecular geometry of ethers 1a-h: The optimized molecular structure of aryl 1-(2,4-dinitronaphthyl) ethers 1a-h are compared with phenyl 1-naphthyl ether (NPE) 4 which are calculated by B3LYP/6-311G (d, p) level. Such calculation is a step to know the reactivity of these ethers as precursors to study nucleophilic substitution reactions involving regioselectivity between ipso naphthyl center and ipso aryl center. Also, we use these theoretical results to compare the molecular structure and nature of substituted ether 1b-h with unsubstituted ether 1a and phenyl 1-naphthyl ether 4 and amine 5.

Optimized geometry of phenyl 1-naphthyl ether (NPE) 4: The results of B3LYP/6-311G (d, p) calculations and the numbering of atoms for the optimized geometrical parameters (bond length, angles and dihedral angles and atomic charges) of phenyl 1-naphthyl ether 4 are listed Table 1 and shown in Figure 2.

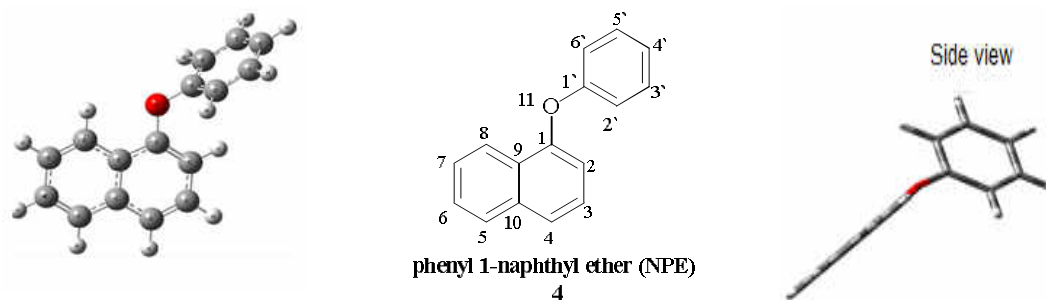


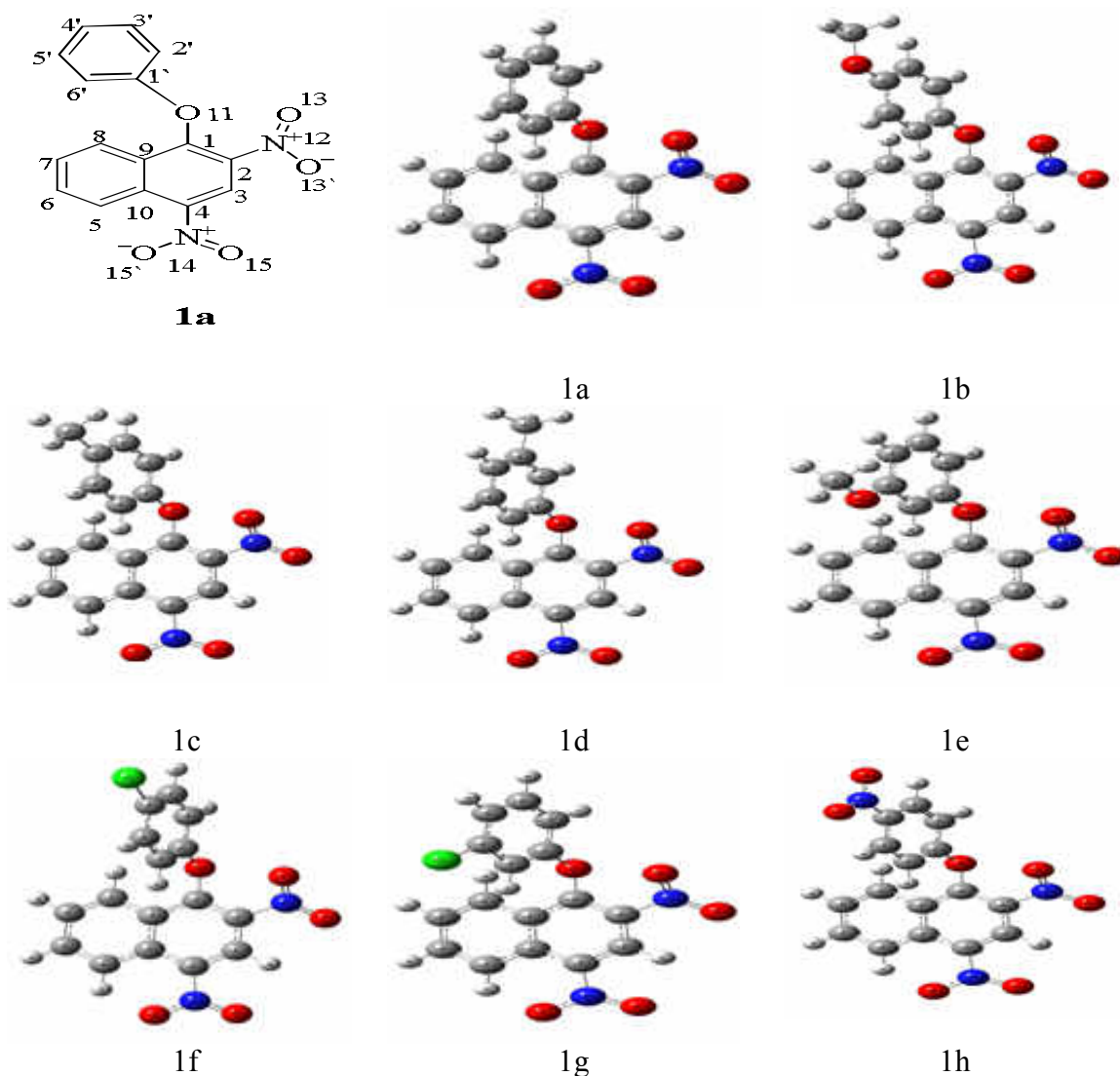
Figure 2. Optimized structure of phenyl 1-naphthylether 4 with numbering of atoms

Table 1. Geometrical parameters of some phenyl-naphthyl ether 4 obtained by B3LYP/6-311G density functional calculations

Bond Length (Å)	B3LYP/6-311 G(d,p)	Bond angles (°)	B3LYP/6-311 G(d,p)	Dihedral angles (°)	B3LYP/6-311 G(d,p)
C ₁ -O ₁₁	1.378	C ₁ -O ₁₁ -C _{1'}	120.4°	C ₂ -C ₁ -O ₁₁ -C _{1'}	-14.50°
C _{1'} -O ₁₁	1.387	O ₁₁ -C ₁ -C ₂	123.9°	C ₆ -C ₁ -O ₁₁ -C _{1'}	167.20°

Table 1 shows that bond lengths of C₁-O₁₁ and C_{1'}-O₁₁ are slightly different presumably due to the delocalization of the lone pair of electrons on O₁₁ with the phenyl ring which it is less pronounced than does with the naphthyl ring. While dihedral angles C₂-C₁-O₁₁-C_{1'} and C₆-C₁-O₁₁-C_{1'} and side view, Figure 2 of 4 suggest that the phenyl and naphthyl rings are not planar. The Milliken atomic charges of atoms of compound 4 showed that all the aromatic carbon atoms are negatively charged except C₁ and C_{1'} are electropositive (0.163 and 0.103 respectively) because they bonded to the more electronegative O-atom. The more positive charge density on C₁ than C_{1'} pointing out that C₁ is of greater electrophilicity than C_{1'}.

Molecular structure and optimized geometry of aryl 1-(2,4-dinitronaphthyl) ethers 1a-h: The calculated bond length, angles and dihedral angles and the numbering of atoms for the optimized geometries of aryl 1-(2,4-dinitronaphthyl) ethers 1a-h using B3LYP/6-311G(d,p) are listed in Table 2 and shown in Figure 3. To the best of our knowledge, only the unsubstituted ether 1a, (X=H) is previously prepared (13) and the geometric structures of substituted ethers 1b-h are not available in the literature. Table 2 shows that bond distances and bond angles of aryl 1-(2,4-dinitronaphthyl) ethers 1a-h are slightly changed with changing in substituent located at para and meta positions of aryl ring.

**Figure 3. Molecular model of aryl 1-(2,4-dinitronaphthyl) ethers 1a-h with numbering of atoms.**

Bond Length: The B3LYP/6-311G(d,p) calculation of C₁-O₁₁, C_{1'}-O₁₁, C₁-C₂, C₂-C₃ and C_{1'}-O₁₁ in 1a-h compared to the same bond lengths in phenyl 1-naphthyl ether 4 indicates that the presence of two nitro groups located in 2 and 4-positions in 1a elongate C₁-C₂ (1.384 Å), C_{1'}-O₁₁ (1.394 Å) and shorten C₁-O₁₁ (1.360 Å). This is presumably due to the expected resonance between the lone pair of ether linkage O₁₁ with the two nitro groups at positions 2 and 4.

The small change in C_1-O_{11} and $C_{1'}-O_{11}$ bond lengths by introduction of either EDG or EWG at positions 3- and 4- in the phenyl ring, C_1-O_{11} and $C_{1'}-O_{11}$ bond lengths are explained by their poor electronic effect. The lone pair of the etheric oxygen for compound 1h, ($X=4\text{-NO}_2$) is engaged in two cross conjugations either with the 2,4-dinitronaphthyl group or with the 4-nitrophenyl group. However, the resonance is pronounced between lone pair of O_{11} and 2,4-dinitronaphthyl ring more than with 4-nitrophenyl as indicated from the larger single bond character of $C_{1'}-O_{11}$ relative to C_1-O_{11} in compound 1a, ($X=H$), Table 2 as shown in Figure 4. Table 2 shows that the bond lengths C_1-O_{11} and $C_{1'}-O_{11}$ in general is slightly increase by the presence of EWG and decreases by EDG and the latter bond lengths are longer than the former bonds. Accordingly, the attack of a nucleophile on the ipso carbon of aryl ring $C_{1'}$ is more likely and 2,4-dinitronaphthoxide ion is possibly the leaving group.

Bond angles: The calculated bond angles of $C_1-O_{11}-C_{1'}$ for all substituent are nearly equal and the difference between them is not exceeding 0.3\AA . As a result, the electrophilic centers C_1 and $C_{1'}$ are interacting equally with the same nucleophile, **Table 2**.

Table 2. Optimized geometrical parameters, some bond length and bond angles of aryl 1-(2,4-dinitronaphthyl) ethers 1a-h calculated by B3LYP/6-311G (d, p) density functional method

Bond Length	1a	1b	1c	1d	1e	1f	1g	1h
C_1-O_{11}	1.360	1.358	1.359	1.359	1.360	1.362	1.363	1.367
$C_{1'}-O_{11}$	1.394	1.399	1.396	1.396	1.394	1.391	1.389	1.381
Bond angles ($^\circ$)								
$C_1-O_{11}-C_{1'}$	121.3 $^\circ$	121.1 $^\circ$	121.1 $^\circ$	121.3 $^\circ$	121.2 $^\circ$	121.2 $^\circ$	121.3 $^\circ$	121.4 $^\circ$
$O_{11}-C_1-C_2$	121.8 $^\circ$	121.0 $^\circ$	121.6 $^\circ$	121.9 $^\circ$	122.1 $^\circ$	122.0 $^\circ$	122.1 $^\circ$	122.0 $^\circ$
Dihedral angle ($^\circ$)								
$C_{1'}-O_{11}-C_1-C_2$	-98.2 $^\circ$	-104.7 $^\circ$	-99.4 $^\circ$	-97.2 $^\circ$	-94.8 $^\circ$	-94.5 $^\circ$	-92.6 $^\circ$	99.4 $^\circ$
$C_{1'}-O_{11}-C_1-C_9$	88.3 $^\circ$	82.0 $^\circ$	87.0 $^\circ$	89.3 $^\circ$	91.4 $^\circ$	91.7 $^\circ$	93.6 $^\circ$	94.0 $^\circ$
$C_2-C_{1'}-O_{11}-C_1$	1.8 $^\circ$	12.0 $^\circ$	3.3 $^\circ$	-0.78 $^\circ$	-3.6 $^\circ$	-2.2 $^\circ$	-7.3 $^\circ$	-4.0 $^\circ$
$C_6-C_{1'}-O_{11}-C_1$	177.7	168.8	176.5 $^\circ$	-179.9	177.3 $^\circ$	178.6 $^\circ$	174.0	177.2 $^\circ$

Dihedral angles: The optimized geometry of ethers 1a-h shown in the side and front views, Figure 5, for example 1a, is consistent with the dihedral angles $C_2-C_1-O_{11}-C_{1'}$ and $C_2-C_{1'}-O_{11}-C_1$ are non-planar geometry in which the phenyl ring is deviates from the plane of naphthyl ring.

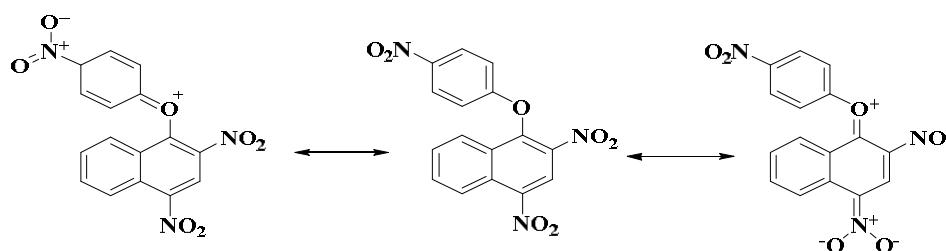


Figure 4. Resonance structures of 4-nitrophenyl 1-(2,4-dinitronaphthyl) ethers 1h.

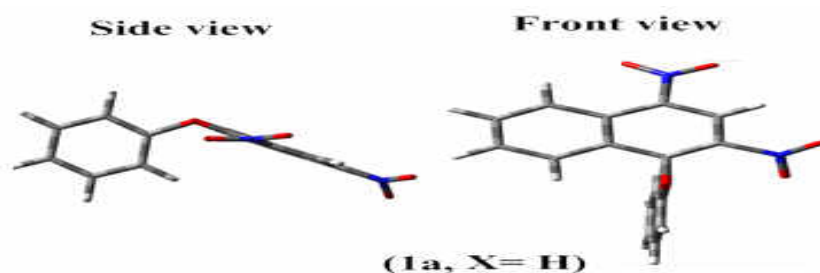


Figure 5. The optimized geometry of ethers 1a-h shown in the side and front views

Table 3. Mulliken, NBO atomic charge and atomic orbital coefficient of LUMO for the selected centers (C_1 , $C_{1'}$) calculated by B3LYP/6-311G (d, p) for aryl 2,4-dinitronaphthalene ethers 1a-h.

Mulliken atomic charges								
Atom	1a	1b	1c	1d	1e	1f	1g	1h
C_1	0.170	0.177	0.171	0.171	0.162	0.163	0.156	0.155
$C_{1'}$	0.162	0.138	0.161	0.170	0.171	0.168	0.167	0.189
NBO atomic charges								
C_1	0.382	0.383	0.383	0.384	0.384	0.378	0.377	0.371
$C_{1'}$	0.324	0.290	0.315	0.334	0.342	0.322	0.344	0.355
Atomic Orbital Coefficient of LUMO								
C_1	0.1912	0.1869	0.1900	0.1915	0.1928	0.1941	0.1950	0.1966
$C_{1'}$	0.0078	0.0078	0.0079	0.0078	0.0078	0.0077	0.0076	0.0071

Table 2 shows that the calculated values of the dihedral angles $C_{11}-O_{11}-C_1-C_2$, $C_{11}-O_{11}-C_1-C_9$, $C_2-C_{11}-O_{11}-C_1$ and $C_6-C_{11}-O_{11}-C_1$ for most ethers 1a-h indicated a non-planarity of aryl and naphthyl rings. A conformation may have steric hindrance with the 2-nitro group, so it may reduce the ability of fast attack by nucleophiles from the front side. The calculated effective atomic charges namely Mulliken and Natural Bond Orbital (NBO)(14) and the atomic orbital coefficient of LUMO using B3LYP level with 6-311G(d,p) basis set for the compounds 1a-h are given in Table 3(15). Both the Mulliken and NBO charges show that the naphthyl ipso carbon C_1 is more positively charged than the aryl ipso carbon C_{11} , and slightly depends on the nature and position of substituent in the aryl moiety. Thus the atomic charge factor is important in determining the reactivity of these centers toward nucleophilic attack. The general inspection of the coefficient on the naphthyl ipso carbon and the aryl ipso carbon atom shows that its value is greater for C_1 compared to C_{11} . This indicates that the interaction of a nucleophile with the naphthyl ipso carbon C_1 is controlled by its charge, while the reaction of the nucleophile with the aryl ipso carbon C_{11} would be controlled by its coefficient. Thus C_{11} can be considered as the high hard electrophilic center while C_1 is the least one.

Table 4 shows that the experimental IR vibrational and the theoretical wave numbers values calculated by B3LYP/6-311G (d, p) method are in good agreement with experimental wave numbers. The weak peaks in the region $3068-3087\text{ cm}^{-1}$ correspond to the aromatic $sp^2=C-H$, while the NO_2 (16) group exhibited two strong absorption peaks for asymmetric and symmetric stretching at ranges $1540-1625\text{ cm}^{-1}$ and $1360-1400\text{ cm}^{-1}$, respectively. It has been reported that the (C-O-C) bond(17) showed two medium intensity peaks at ranges $1116-1268\text{ cm}^{-1}$ and $950-1107\text{ cm}^{-1}$ due to the asymmetric and symmetric stretching vibrational peaks, respectively. The calculated frequencies of (C_1-O-C_{11}) and NO_2 peaks are of higher value than those observed values for the majority of the normal modes.

(C-O) vibrations, (C-O-C) vibrations: The stretching vibrations of ($O_{11}-C_1$) and ($C_{11}-O_{11}$) groups have already been reported at 1270 cm^{-1} and 1040 cm^{-1} respectively.(18) In the present study, the experimental stretching peaks of the corresponding groups are observed at $1116-1268$ and $950-1170\text{ cm}^{-1}$ (strong to medium intensity). The calculated ($O_{11}-C_1$) frequency in naphthyl group is at $1244-1252\text{ cm}^{-1}$. On the other hand, the stretching vibrations of ($O_{11}-C_{11}$ aryl) peaks are calculated at $1157-1262\text{ cm}^{-1}$ depending on the substituents in the aryl moiety, Table 4.

Table 4. Experimental and Calculated B3LYP/6-311G (d, p) level vibrational frequencies (cm^{-1}) of 2,4-dinitronaphthalene aryl ethers 1a-h

	1a	1b	1c	1d	1e	1f	1g	1h
$U_{\text{STRECH}} (\text{cm}^{-1})$	Calculated values							
$C_{11}-O_{11}$	1251	1248	1252	1244	1246	1252	1251	1252
$C_{11}-O_{11}$	1251	1203	1222	1262	1157	1252	1251	1252
$N_{12}-O_{13}$	1364	1365	1364	1363	1364	1365	1365	1366
$N_{12}-O_{13}$	1593	1595	1594	1593	1594	1592	1593	1595
$N_{14}-O_{15}$	1364	1365	1364	1364	1364	1365	1365	1366
$N_{14}-O_{15}$	1600	1600	1600	1600	1600	1601	1601	1603
C_2-N_{12}	935	936	935	929	930	934	935	934
C_4-N_{14}	1003	1004	1003	1002	1003	1003	1003	1002
$U_{\text{BENDING}} (\text{cm}^{-1})$								
$O_{13}-N_{12}-O_{13}$	935	936	935	929	930	934	935	934
$O_{15}-N_{14}-O_{15}$	872	875	875	874	870	873	803	865
$U_{\text{STRECH}} (\text{cm}^{-1})$	Experimental values							
$C_{11}-O_{11}-C_{11}$ asym	1209	1231	1268	1207	1241	1116	1268	1232
$C_{11}-O_{11}-C_{11}$ sym	1041	1025	1083	962	1085	950	1085	1107
NO_2 asym	1539	1532	1530	1541	1530	1535	1528	1528
NO_2 sym	1359	1339	1347	1359	1415	1346	1341	1344
C_2-N_{12}	750	830	767	777	835	755	830	839
C_4-N_{14}	962	905	950	962	892	905	890	889

Table 5. The $sp^2=C-H$ stretching vibrations of naphthalene ring in 1a-h.

Bonds	Calculated values							
	$\nu_{\text{STRECH}} (\text{cm}^{-1}), sp^2=C-H (\text{ArH})$							
	1a	1b	1c	1d	1e	1f	1g	1h
C_3-H_3	3240	3239	3240	3240	3242	3240	3241	3240
C_5-H_5	3250	3250	3251	3251	3250	3250	3250	3251
C_6-H_6	3192	3192	3192	3192	3192	3192	3193	3194
C_7-H_7	3192	3192	3192	3192	3193	3193	3193	3194
C_8-H_8	3221	3221	3221	3220	3220	3220	3220	3220
$C_{21}-H_{21}$	3201	3204	3197	3201	3209	3209	3216	3202
$C_{31}-H_{31}$	3198	3204	3167	3201	-	3210	-	3226
$C_{41}-H_{41}$	3201	-	-	3182	3214	-	3212	-
$C_{51}-H_{51}$	3201	3210	3163	-	3177	3210	3212	3228
$C_{61}-H_{61}$	3201	3210	3197	3184	3208	3210	3212	3205
	Experimental values							
	$\nu_{\text{STRECH}} (\text{cm}^{-1})$							
$sp^2=C-H (\text{ArH})$	3084	3085	3075	3068	3086	3078	3084	3087

Nitro group vibrations: Nitro groups have strong absorption due to their asymmetric and symmetric vibrations at $1540-1625\text{ cm}^{-1}$ and $1360-1400\text{ cm}^{-1}$ respectively.(15)

Table 6. Experimental and Calculated electronic transition properties for ethers 1a-h by TD-DFT/ B3LYP/ 6-311G (d, p) in DMSO

Cpds	Experimental λ_{max}	Theoretical λ_{max}	Oscillator strength(f)	Assignment of electronic transition	Electronic transition type
1a	366 nm	377 nm	0.131	HOMO-1-LUMO	$\pi \rightarrow \pi^*$
	346 nm	350 nm	0.032	HOMO-1-LUMO+1	$\pi \rightarrow \pi^*$
	303 nm	302 nm	0.026	HOMO-3-LUMO	$\pi \rightarrow \pi^*$
	290 nm	284 nm	0.030	HOMO-3-LUMO	$\pi \rightarrow \pi^*$
1b	362 nm	377 nm	0.146	HOMO-1-LUMO	$\pi \rightarrow \pi^*$
	308 nm	352 nm	0.051	HOMO-2-LUMO+1	$\pi \rightarrow \pi^*$
	304 nm	321 nm	0.088	HOMO-3-LUMO	$\pi \rightarrow \pi^*$
	298 nm	304 nm	0.034	HOMO-2-LUMO+1	$\pi \rightarrow \pi^*$
1c	364 nm	377 nm	0.139	HOMO-1-LUMO	$\pi \rightarrow \pi^*$
	313 nm	351 nm	0.159	HOMO-1-LUMO+1	$\pi \rightarrow \pi^*$
	302 nm	321 nm	0.079	HOMO-2-LUMO	$\pi \rightarrow \pi^*$
	282 nm	302 nm	0.069	HOMO-2-LUMO	$\pi \rightarrow \pi^*$
1d	367 nm	376 nm	0.072	HOMO-1-LUMO	$n \rightarrow \pi^*$
	316 nm	351 nm	0.046	HOMO-1-LUMO-1	$\pi \rightarrow \pi^*$
	301 nm	302 nm	0.063	HOMO-3-LUMO	$\pi \rightarrow \pi^*$
	278 nm	285 nm	0.040	HOMO-3-LUMO+1	$\pi \rightarrow \pi^*$
1e	360 nm	375 nm	0.112	HOMO-2-LUMO	$\pi \rightarrow \pi^*$
	345 nm	321 nm	0.069	HOMO-3-LUMO	$\pi \rightarrow \pi^*$
	304 nm	303 nm	0.090	HOMO-3-LUMO	$\pi \rightarrow \pi^*$
	295 nm	291 nm	0.010	HOMO-LUMO+1	$n \rightarrow \pi^*$
1f	361 nm	377 nm	0.125	HOMO-1-LUMO	$\pi \rightarrow \pi^*$
	312 nm	319 nm	0.044	HOMO-2-LUMO	$\pi \rightarrow \pi^*$
	300 nm	302 nm	0.078	HOMO-3-LUMO	$\pi \rightarrow \pi^*$
	279 nm	284 nm	0.035	HOMO-2-LUMO	$\pi \rightarrow \pi^*$
1g	363 nm	378 nm	0.126	HOMO-1-LUMO	$\pi \rightarrow \pi^*$
	316 nm	321 nm	0.079	HOMO-3-LUMO	$\pi \rightarrow \pi^*$
	304 nm	302 nm	0.086	HOMO-3-LUMO	$\pi \rightarrow \pi^*$
	274 nm	285 nm	0.017	HOMO-3-LUMO+1	$\pi \rightarrow \pi^*$
1h	445 nm	381 nm	0.131	HOMO-LUMO	$n \rightarrow \pi^*$
	373 nm	351 nm	0.049	HOMO-LUMO+1	$n \rightarrow \pi^*$
	301 nm	308 nm	0.049	HOMO-2-LUMO	$\pi \rightarrow \pi^*$
	291 nm	300 nm	0.070	HOMO-3-LUMO	$\pi \rightarrow \pi^*$

Table 7. Experimental and Calculated electronic transition properties for ethers 1a-h by TD-DFT/ CAM-B3LYP/ 6-311G (d, p) in DMSO

Cpds	Experimental λ_{max}	Theoretical λ_{max}	Oscillator strength(f)	Assignment of electronic transition	Electronic transition type
1a	366 nm	377 nm	0.183	HOMO-LUMO	$n \rightarrow \pi^*$
	346 nm	350 nm	0.032	HOMO-5-LUMO	$\pi \rightarrow \pi^*$
	303 nm	302 nm	0.026	HOMO-5-LUMO+1	$\pi \rightarrow \pi^*$
	290 nm	284 nm	0.030	HOMO-6-LUMO+2	$\pi \rightarrow \pi^*$
1b	362 nm	377 nm	0.187	HOMO-1-LUMO	$\pi \rightarrow \pi^*$
	308 nm	352 nm	0.035	HOMO-6-LUMO	$\pi \rightarrow \pi^*$
	304 nm	321 nm	0.029	HOMO-6-LUMO+1	$\pi \rightarrow \pi^*$
	298 nm	304 nm	0.015	HOMO-1-LUMO+1	$\pi \rightarrow \pi^*$
1c	364 nm	377 nm	0.033	HOMO-LUMO	$n \rightarrow \pi^*$
	313 nm	351 nm	0.159	HOMO-1-LUMO	$\pi \rightarrow \pi^*$
	302 nm	321 nm	0.034	HOMO-5-LUMO	$\pi \rightarrow \pi^*$
	282 nm	302 nm	0.029	HOMO-5-LUMO+1	$\pi \rightarrow \pi^*$
1d	367 nm	376 nm	0.180	HOMO-LUMO	$n \rightarrow \pi^*$
	316 nm	351 nm	0.033	HOMO-5-LUMO	$\pi \rightarrow \pi^*$
	301 nm	302 nm	0.025	HOMO-5-LUMO+1	$\pi \rightarrow \pi^*$
	278 nm	285 nm	0.036	HOMO-6-LUMO+1	$\pi \rightarrow \pi^*$
1e	360 nm	375 nm	0.182	HOMO-1-LUMO	$\pi \rightarrow \pi^*$
	345 nm	321 nm	0.031	HOMO-4-LUMO+1	$\pi \rightarrow \pi^*$
	304 nm	303 nm	0.016	HOMO-4-LUMO	$\pi \rightarrow \pi^*$
	295 nm	291 nm	0.023	HOMO-2-LUMO	$\pi \rightarrow \pi^{**}$
1f	361 nm	377 nm	0.186	HOMO-LUMO	$n \rightarrow \pi^*$
	312 nm	319 nm	0.030	HOMO-5-LUMO	$\pi \rightarrow \pi^*$
	300 nm	302 nm	0.026	HOMO-5-LUMO+1	$\pi \rightarrow \pi^*$
	279 nm	284 nm	0.017	HOMO-1-LUMO+1	$\pi \rightarrow \pi^*$
1g	363 nm	378 nm	0.181	HOMO-LUMO	$n \rightarrow \pi^*$
	316 nm	321 nm	0.029	HOMO-5-LUMO	$\pi \rightarrow \pi^*$
	304 nm	302 nm	0.016	HOMO-1-LUMO	$\pi \rightarrow \pi^*$
	274 nm	285 nm	0.017	HOMO-LUMO+1	$n \rightarrow \pi^*$
1h	445 nm	381 nm	0.201	HOMO-LUMO	$n \rightarrow \pi^*$
	373 nm	351 nm	0.026	HOMO-6-LUMO	$\pi \rightarrow \pi^*$
	301 nm	308 nm	0.022	HOMO-6-LUMO+1	$\pi \rightarrow \pi^*$
	291 nm	300 nm	0.015	HOMO-LUMO+1	$n \rightarrow \pi^*$

Experimentally, strong IR absorptions due to asymmetric stretching vibrations of the NO₂ group are found at 1528-1541 cm⁻¹. While, the very intense peak corresponding to the symmetric stretching mode of the NO₂ groups mixed with ring stretching vibrations appear in IR at 1339-1415 cm⁻¹ while the observed asymmetric and symmetric vibrations of the nitro group at 1592-1603 cm⁻¹ and 1364-1366 cm⁻¹ respectively. The intensity enhancement of these wave numbers is due to conjugation with the aromatic ring. Therefore, there are similar absorption values between experimental and computed values, Table 4.

Table 8. Experimental and Calculated electronic transition properties for ethers 1a-h by TD-DFT/ CAM-B3LYP/ 6-311++G (d, p) in DMSO

Cpds	Experimental λ_{\max}	Theoretical λ_{\max}	Oscillator strength h(f)	Assignment of electronic transition	Electronic transition type
1a	366 nm	340 nm	0.194	HOMO-1-LUMO	$n \rightarrow \pi^*$
	346 nm	316 nm	0.054	HOMO-1-LUMO+1	$\pi \rightarrow \pi^*$
	303 nm	306 nm	0.027	HOMO-3-LUMO	$\pi \rightarrow \pi^*$
	290 nm	278 nm	0.030	HOMO-3-LUMO	$\pi \rightarrow \pi^*$
1b	362 nm	340 nm	0.208	HOMO-1-LUMO	$n \rightarrow \pi^*$
	308 nm	317 nm	0.062	HOMO-1-LUMO+1	$\pi \rightarrow \pi^*$
	304 nm	308 nm	0.027	HOMO-2-LUMO	$\pi \rightarrow \pi^*$
	298 nm	297 nm	0.012	HOMO-LUMO+1	$n \rightarrow \pi^*$
1c	364 nm	339 nm	0.184	HOMO-1-LUMO	$\pi \rightarrow \pi^*$
	313 nm	316 nm	0.057	HOMO-1-LUMO+1	$\pi \rightarrow \pi^*$
	302 nm	308 nm	0.025	HOMO-3-LUMO	$\pi \rightarrow \pi^*$
	282 nm	281 nm	0.009	HOMO-3-LUMO	$\pi \rightarrow \pi^*$
1d	367 nm	341 nm	0.183	HOMO-1-LUMO	$\pi \rightarrow \pi^*$
	316 nm	316 nm	0.055	HOMO-1-LUMO-1	$\pi \rightarrow \pi^*$
	301 nm	308 nm	0.025	HOMO-3-LUMO	$\pi \rightarrow \pi^*$
	278 nm	279 nm	0.094	HOMO-2-LUMO	$\pi \rightarrow \pi^*$
1e	360 nm	341 nm	0.192	HOMO-1-LUMO	$\pi \rightarrow \pi^*$
	345 nm	316 nm	0.050	HOMO-1-LUMO+1	$\pi \rightarrow \pi^*$
	304 nm	310 nm	0.013	HOMO-3-LUMO+1	$\pi \rightarrow \pi^*$
	295 nm	299 nm	0.025	HOMO-2-LUMO+1	$\pi \rightarrow \pi^*$
1f	361 nm	390 nm	0.119	HOMO-1-LUMO	$\pi \rightarrow \pi^*$
	312 nm	367 nm	0.056	HOMO-1-LUMO+1	$\pi \rightarrow \pi^*$
	300 nm	326 nm	0.013	HOMO-3-LUMO	$\pi \rightarrow \pi^*$
	279 nm	-	-	-	-
1g	363 nm	341 nm	0.192	HOMO-1-LUMO	$\pi \rightarrow \pi^*$
	316 nm	316 nm	0.046	HOMO-1-LUMO+1	$\pi \rightarrow \pi^*$
	304 nm	308 nm	0.026	HOMO-3-LUMO+1	$\pi \rightarrow \pi^*$
	274 nm	278 nm	0.125	HOMO-3-LUMO	$\pi \rightarrow \pi^*$
1h	445 nm	340 nm	0.215	HOMO-LUMO	$n \rightarrow \pi^*$
	373 nm	315 nm	0.043	HOMO-LUMO+1	$n \rightarrow \pi^*$
	301 nm	309 nm	0.026	HOMO-2-LUMO+1	$\pi \rightarrow \pi^*$
	291 nm	291 nm	0.021	HOMO-1-LUMO	$\pi \rightarrow \pi^*$

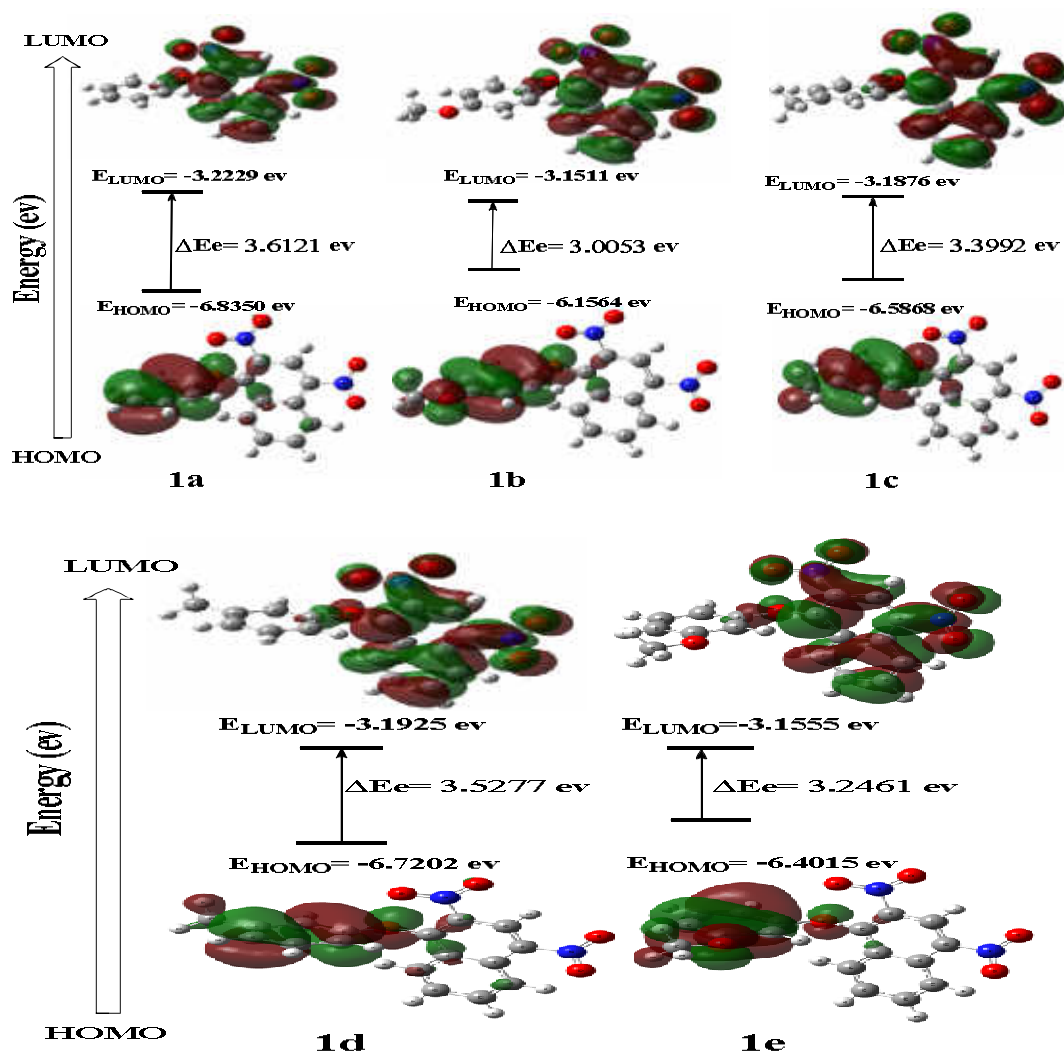
(C-H) vibrations: The $sp^2=C-H$ (aromatic) stretching vibrations occur in the region (19) $3200-3000\text{ cm}^{-1}$. Actually, the $sp^2=C-H$ (aromatic) stretching peak in ethers 1a-h are observed at $3068-3087\text{ cm}^{-1}$ in FT-IR spectrum. This peak is nearly matching with the calculated value at $3177-3251\text{ cm}^{-1}$. Ethers 1a-h have five adjacent C-H moieties with two fused benzene rings and the expected five C-H stretching vibrations are C_3-H_3 , C_5-H_5 , C_6-H_6 , C_7-H_7 and C_8-H_8 slightly changed in frequency values and occurred in range of region $3192-3251\text{ cm}^{-1}$. Accordingly, the symmetric stretching vibrations and the asymmetric stretching vibrations, in ethers 1a-h for C_2-H_2 , C_3-H_3 , C_4-H_4 , C_5-H_5 , C_6-H_6 bonds have great change in values and occur in range of region $3163-3228\text{ cm}^{-1}$, Table 5. Three factors may be responsible for the discrepancies between the experimental and computed spectra: The first is the fact that the experimental value is unharmonic frequency while the calculated value is a harmonic frequency and the second reason caused by the environment (20). The third reason is that the calculations have been actual done on a single molecule while the experimental values recorded in the presence of intermolecular interactions.

Experimental and Theoretical UV-Visible analysis of 1a-h: All the structures of ethers 1a-h allow strong $\pi \rightarrow \pi^*$ and $\sigma \rightarrow \sigma^*$ transition in the UV-VIS region with high extinction coefficients (21). The vertical excitation energies, oscillator strength f and wavelength are calculated using various bases sets namely TD-DFT/ B3LYP/ 6-311G (d,p), TD-DFT/ CAM-B3LYP/ 6-311G (d,p) and TD-DFT/ CAM-B3LYP/ 6-311G++(d,p) in DMSO and the measured experimental wavelength are tabulated in Table 6-8. The use of TD-DFT/B3LYP/6-311G (d, p) bases set indicates that the calculated absorption maxima values have been found to be at $\lambda = 381-375\text{ nm}$ while the corresponding experimental value is at $\lambda = 445-360\text{ nm}$. The range of transition observed at $\lambda = 381\text{ nm}$ is $f = 0.131$ and that at $\lambda = 275\text{ nm}$ is $f = 0.112$, Table 6. The calculated absorption maxima values by using TD-DFT/ CAM-B3LYP/ 6-311G (d,p) basis set in DMSO are absorbed at $\lambda = 381-375\text{ nm}$ while the corresponding experimental value is at $\lambda = 445-360\text{ nm}$. The range of transition observed at $\lambda = 381\text{ nm}$ and at $\lambda = 375\text{ nm}$ are $f = 0.201$ and $f = 0.182$ respectively, Table 7. The TD-DFT/ CAM-B3LYP/ 6-311G++(d,p) basis set in DMSO tabulated in Table 8 reveals that the calculated absorption maxima values are found to be at $\lambda = 390-339\text{ nm}$ while that the corresponding experimental value is at $\lambda = 445-360\text{ nm}$. The range of transitions are observed at $\lambda = 390\text{ nm}$ is $f = 0.119$ and at $\lambda = 339\text{ nm}$ is $f = 0.184$. The theoretical results indicate that the density functional B3LYP methods TD-DFT/ B3LYP/ 6-311G (d, p), TD-DFT/ CAM-B3LYP/ 6-311G (d, p) provide satisfactory results to predict UV properties, Table 6, 7. The HOMO-LUMO gap can be used to predict the shift of absorbance where HOMO-LUMO gap of unsubstituted compound 1a, (X= H) is found to be higher than those of the substituted one except for the p-nitro substituent 1h, (X= 4-NO₂). This implies that it is easier to promote an electron from the HOMO to the LUMO by substituting electron donating and withdrawing groups and will result in a red shift of the absorption spectrum.

Experimental and Theoretical ¹H NMR Analysis Spectra of 1a-h: The measured ¹H NMR spectra of aryl 1-(2,4-dinitronaphthyl) ethers 1a-h showed singlet signal of naphthalene H₃ in range $\delta 8.44-8.90\text{ ppm}$, while H₅ and H₈ appeared as two doublets in all compounds in range $\delta 8.21-8.72\text{ ppm}$, except in 4-nitro derivative 1h in which H₈ appeared as one multiplet at the range $\delta 8.21-8.23\text{ ppm}$.

Table 9. Theoretical and experimental ¹H chemical shift (ppm) of 1a-h

Cpds	Proton Basis sets	H ₃	H ₅	H ₆	H ₇	H ₈	H _{2'}	H _{3'}	H _{4'}	H _{5'}	H _{6'}	notes
		1a, X = H	B3LYP/6-311g (d, p)	9.909	9.965	8.862	8.592	9.148	6.690	7.975	7.963	
	B3LYP/6-311++g (d, p)	10.085	10.054	9.035	8.687	9.275	6.797	8.184	8.110	8.431	8.434	-
	BLYP/6-311g (d, p)	9.696	9.939	8.920	8.689	9.196	6.856	8.079	8.058	8.470	8.317	-
	Experimental data	8.947	8.526	8.031	7.844	8.215	6.968	7.326	7.102	7.326	6.968	-
1b, X = 4-OCH ₃	B3LYP/6-311g (d, p)	9.823	9.954	8.841	8.552	9.099	6.746	7.478	-	7.598	8.277	OCH ₃ = 4.464
	B3LYP/6-311++g (d, p)	10.393	10.005	8.880	8.584	9.139	6.861	7.616	-	7.743	8.348	OCH ₃ = 4.556
	BLYP/6-311g (d, p)	9.628	9.938	8.835	8.589	9.158	6.822	7.444	-	7.573	8.217	OCH ₃ = 4.831
	Experimental data	8.844	8.721	7.926	7.747	8.402	6.807	6.807	-	6.807	6.807	OCH ₃ = 3.764
1c, X = 4-CH ₃	B3LYP/6-311g (d, p)	9.883	9.962	8.862	8.576	9.126	6.536	7.732	-	8.280	8.261	CH ₃ = 2.978
	B3LYP/6-311++g (d, p)	10.100	10.047	8.923	8.610	9.188	6.641	7.859	-	8.289	8.340	CH ₃ = 3.056
	BLYP/6-311g (d, p)	9.690	9.949	8.865	8.619	9.156	6.646	7.806	-	8.298	8.215	CH ₃ = 3.261
	Experimental data	8.867	8.723	7.937	7.739	8.380	6.756	7.099	-	7.099	6.756	CH ₃ = 2.304
1d, X = 3-CH ₃	B3LYP/6-311g (d, p)	9.916	9.958	8.862	8.596	9.151	6.439	7.842	7.800	-	8.189	CH ₃ = 3.143
	B3LYP/6-311++g (d, p)	10.094	10.053	8.942	8.679	9.249	6.450	7.956	7.923	-	8.299	CH ₃ = 3.191
	BLYP/6-311g (d, p)	9.721	9.949	8.866	8.638	9.171	6.582	7.905	7.855	-	8.143	CH ₃ = 3.417
	Experimental data	8.882	8.726	7.937	7.742	8.365	6.694	7.178	6.924	-	6.632	CH ₃ = 2.301
1e, X = 3-OCH ₃	B3LYP/6-311g (d, p)	9.947	9.962	8.889	8.625	9.201	6.121	-	7.177	8.272	7.848	OCH ₃ = 3.3073
	B3LYP/6-311++g (d, p)	10.089	10.119	8.968	8.661	9.315	6.249	-	7.332	8.272	7.862	OCH ₃ = 4.421
	BLYP/6-311g (d, p)	9.759	9.944	8.891	8.665	9.213	6.123	-	7.187	8.271	6.123	OCH ₃ = 4.663
	Experimental data	8.881	8.718	7.940	7.746	8.359	6.492	-	6.662	7.182	6.358	OCH ₃ = 3.780
1f, X = 4-Cl	B3LYP/6-311g (d, p)	9.893	9.948	8.891	8.618	9.128	6.577	7.781	-	8.223	8.241	-
	B3LYP/6-311++g (d, p)	10.123	10.057	8.960	8.632	9.224	6.710	7.988	-	8.345	8.331	-
	BLYP/6-311g (d, p)	9.713	9.942	8.899	8.666	9.158	6.713	7.843	-	8.254	8.209	-
	Experimental data	8.879	8.724	7.962	7.769	8.312	6.809	7.271	-	7.271	6.809	-
1g, X = 3-Cl	B3LYP/6-311g (d, p)	9.931	9.973	8.914	8.650	9.153	6.513	-	7.809	8.280	8.171	-
	B3LYP/6-311++g (d, p)	10.121	10.109	9.021	8.726	9.313	6.906	-	8.028	8.385	8.211	-
	BLYP/6-311g (d, p)	9.755	9.959	8.922	8.698	9.184	6.621	-	7.860	8.329	8.130	-
	Experimental data	8.898	8.726	7.959	7.776	8.299	6.880	-	7.111	7.247	6.749	-
1h, X = 4-NO ₂	B3LYP/6-311g (d, p)	9.922	9.966	8.931	8.663	9.137	6.753	8.863	-	9.283	8.377	-
	B3LYP/6-311++g (d, p)	10.123	10.073	8.994	8.659	9.206	6.845	8.999	-	9.421	8.386	-
	BLYP/6-311g (d, p)	9.733	9.953	8.932	8.695	9.138	6.872	8.804	-	9.201	8.317	-
	Experimental data	8.909	8.727	7.998	7.802	8.230	6.987	8.22-8.24	-	8.22-8.24	6.987	-



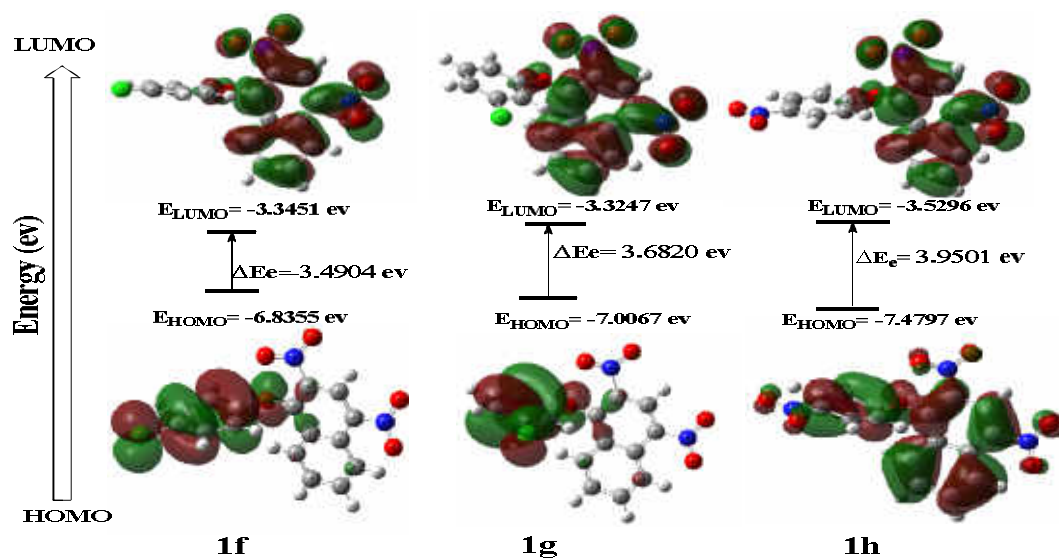


Figure 7. Frontiers molecular orbitals of 1a-h.

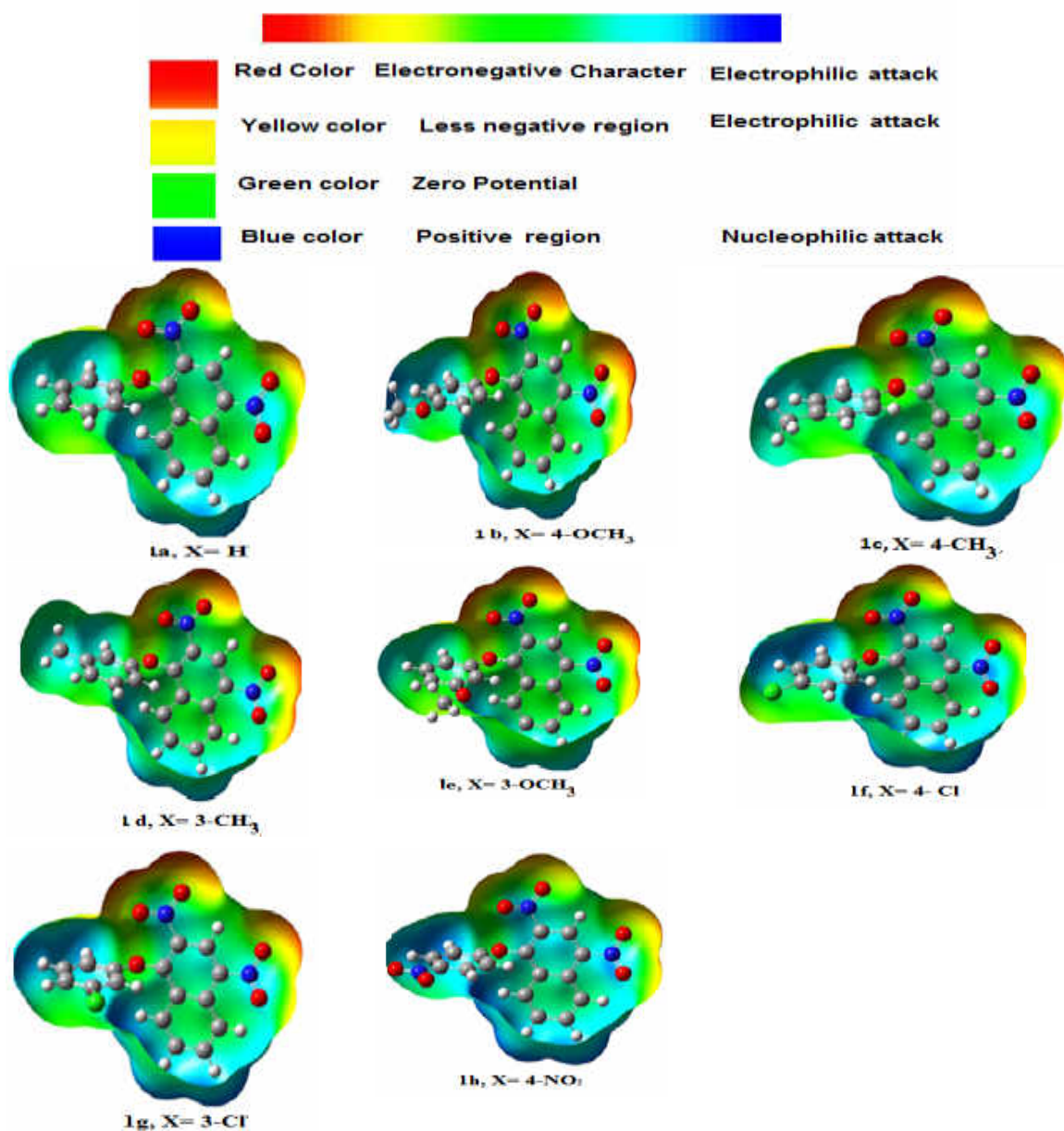


Figure 8. The Total Electron Density surface mapped with Electrostatic Potential of 1a-h.

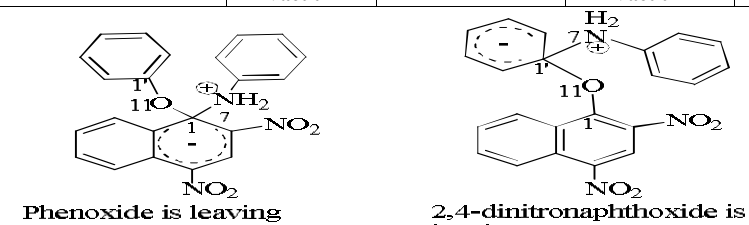
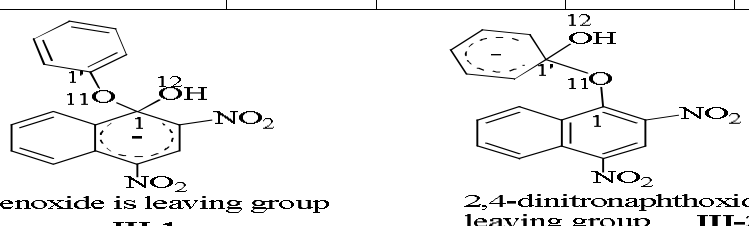
Table 10. Calculated Energies and related molecular values of aryl 2,4-dinitro naphthyl ether 1a-h by B3LYP/6-311G (d, p)

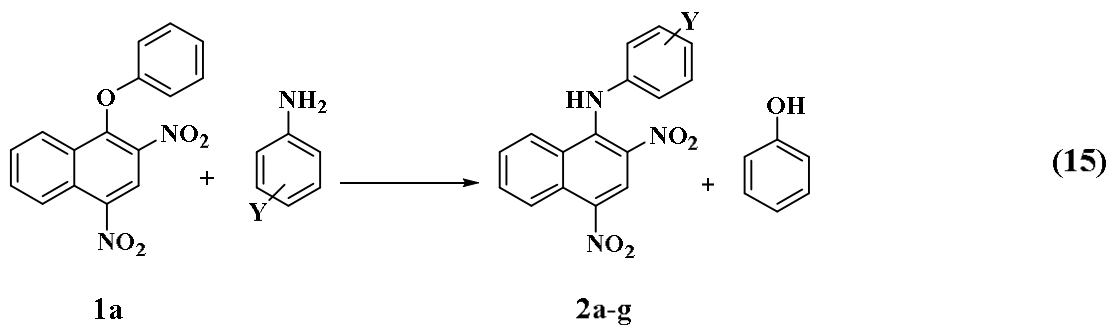
Cpds	1a	1b	1c	1d	1e	1f	1g	1h
	X = H	X = 4-OCH ₃	X = 4-CH ₃	X = 3-CH ₃	X = 3-OCH ₃	X = 4-Cl	X = 3-Cl	X = 4-NO ₂
	0	-0.27	-0.17	-0.07	0.12	0.23	0.37	0.78
E _{HOMO}	-6.86	-6.16	-6.59	-6.72	-6.40	-6.84	-7.00	-7.48
E _{LUMO}	-3.22	-3.15	-3.19	-3.19	-3.16	-3.35	-3.32	-3.53
ΔE _e	3.61	3.00	3.40	3.53	3.25	3.49	3.68	3.95
μ (D)	6.09	7.15	6.39	6.28	6.89	5.35	5.98	6.03
I _p	6.84	6.16	6.59	6.73	6.41	6.84	7.01	7.48
E _A	3.22	3.15	3.19	3.19	3.16	3.35	3.33	3.53
μ (eV)	-5.03	-4.65	-4.89	-4.96	-4.78	-5.09	-5.17	-5.50
χ	5.03	4.65	4.89	4.96	4.78	5.09	5.17	5.50
S	0.55	0.67	0.59	0.57	0.62	0.57	0.54	0.51
η	1.81	1.50	1.70	1.76	1.62	1.75	1.84	1.98
ω	7.00	7.21	7.03	6.96	7.03	7.42	7.25	7.67
ΔN _{max}	2.78	3.10	2.88	2.81	2.94	2.92	2.81	2.79

Table 11. Fukui function (f_k⁺, ω_k⁺ and ω_k⁻ of C₁, C_{1'} in compounds 1a-h.

Cpds	Atom	f ⁺	f	f ⁻	ω _k ⁺	ω _k ⁻
1a	C ₁	-0.00723	0.09213	0.04245	-0.05064	0.64507
	C _{1'}	0.01610	-0.02951	-0.00670	0.11275	-0.20662
1b	C ₁	-0.03443	0.09179	0.02868	-0.24815	0.66149
	C _{1'}	0.04249	-0.03132	0.00559	0.30625	-0.22567
1c	C ₁	-0.02053	0.09220	0.03584	-0.14426	0.64785
	C _{1'}	0.02776	-0.03004	-0.00114	0.19509	-0.21104
1d	C ₁	-0.01553	0.09274	0.03861	-0.11527	0.68845
	C _{1'}	0.01735	-0.02943	-0.00604	0.12879	-0.21846
1e	C ₁	-0.00794	0.09266	0.04236	-0.05797	0.67684
	C _{1'}	0.00209	-0.02803	-0.01297	0.01529	-0.20477
1f	C ₁	-0.01275	0.09338	0.04031	-0.09783	0.71631
	C _{1'}	0.01996	-0.03110	-0.00557	0.15308	-0.23858
1g	C ₁	0.00102	0.09327	0.04714	0.00715	0.65606
	C _{1'}	0.00829	-0.02944	-0.01058	0.05832	-0.20712
1h	C ₁	0.01216	0.08618	0.04917	0.08769	0.62144
	C _{1'}	0.00027	-0.02674	-0.01323	0.00198	-0.19283

Table 12. Bond lengths and Bond angles of the intermediates, for the reaction of ether 1a and aniline in Vacuum

Species	Bond lengths (Å)		Bond angles (°)		Energy in (Hartree/Particle) Vacuum
	BL	Vacuum	BA	Vacuum	
 <p>Phenoxide is leaving group II-1</p> <p>2,4-dinitronaphthoxide is leaving group II-2</p>					
II-1	C ₁ -O ₁₁	1.458	C ₁ -O ₁₁ -C _{1'}	119.9 °	-1380.36357
	C _{1'} -O ₁₁	1.380	O ₁₁ -C ₁ -N ₇	95.7 °	
	C ₁ -N ₇	1.528			
II-2	C ₁ -O ₁₁	1.430	C ₁ -O ₁₁ -C _{1'}	122.4 °	-1380.28462
	C _{1'} -O ₁₁	1.430	O ₁₁ -C ₁ -N ₇	94.9 °	
	C ₁ -N ₇	1.470			
 <p>Phenoxide is leaving group III-1</p> <p>2,4-dinitronaphthoxide is leaving group III-2</p>					
III-1	C ₁ -O ₁₁	1.430	C ₁ -O ₁₁ -C _{1'}	119.9 °	-1170.16202
	C _{1'} -O ₁₁	1.430	O ₁₁ -C ₁ -O ₁₂	102.6 °	
	C ₁ -O ₁₂	1.430			
III-2	C ₁ -O ₁₁	1.430	C ₁ -O ₁₁ -C _{1'}	118.7 °	-1170.05765
	C _{1'} -O ₁₁	1.430	O ₁₁ -C ₁ -O ₁₂	100.6 °	
	C ₁ -O ₁₂	1.430			



a, Y = H; b, Y = 4-OCH₃; c, Y = 4-CH₃; d, Y = 3-CH₃; e, Y = 3-OCH₃; f, Y = 4-Cl;
g, Y = 3-Cl

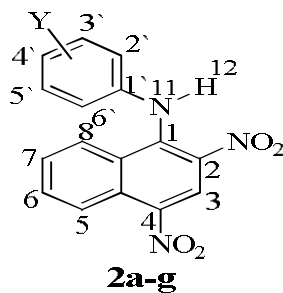


Figure 10. Aryl 2,4-dinitro-1-naphthyl amine 2a-g

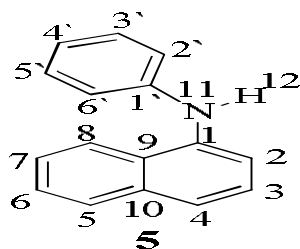


Figure 11. Molecular modeling of N-phenyl-naphthylamine 5 with numbering of atoms

Table 13. Optimized geometrical parameters of N-phenyl 1-naphthylamine 5 obtained by B3LYP/6-311G density functional calculations

Bond Length (Å)	B3LYP/6-311 (d,p)	Bond angles (°)	B3LYP/6-311 G(d,p)	Dihedral angles (°)	B3LYP/ 6-311 G(d,p)
C ₁ -N ₁₁	1.419	C ₁ -N ₁₁ -C _{1'}	124.6°	C ₂ -C ₁ -N ₁₁ -C _{1'}	109.94°
C ₁ -N ₁₁	1.407	N ₁₁ -C ₁ -C ₂	120.1°	C ₉ -C ₁ -N ₁₁ -C _{1'}	-73.34°
C ₁ -C ₂	1.380	N ₁₁ -C ₁ -C ₉	120.1°	C ₂ -C ₁ -N ₁₁ -C ₁	-175.78°
C ₁ -C ₂	1.432	C ₂ -C ₁ -N ₁₁	118.5°	C ₆ -C ₁ -N ₁₁ -C ₁	-4.79°
N ₁₁ -H ₁₂	1.009	C ₆ -C ₁ -N ₁₁	122.8°	C ₂ -C ₁ -N ₁₁ -H ₁₂	-35.37°
		H ₁₂ -N ₁₁ -C ₁	113.5°	C ₉ -C ₁ -N ₁₁ -H ₁₂	-141.35°
		H ₁₂ -N ₁₁ -C _{1'}	113.2°		

Table 14. The Mulliken charge distribution of N-phenyl-naphthylamine 5 obtained by B3LYP/6-311G (d, p) density functional calculations

Atoms	Mulliken	Atoms	Mulliken
H ₂	0.087	C ₁	0.089
H ₃	0.094	C ₂	-0.056
H ₄	0.082	C ₃	-0.098
H ₅	0.084	C ₄	-0.045
H ₆	0.093	C ₅	-0.063
H ₇	0.095	C ₆	-0.085
H ₈	0.109	C ₇	-0.092
H _{2'}	0.086	C ₈	-0.024
H _{3'}	0.090	C ₉	-0.069
H _{4'}	0.088	C ₁₀	-0.055
H _{5'}	0.092	C _{1'}	0.133
H _{6'}	0.115	C _{2'}	-0.104
H ₁₂	0.217	C _{3'}	-0.096
N ₁₁	-0.478	C _{4'}	-0.101
		C _{5'}	-0.098
		C _{6'}	-0.092

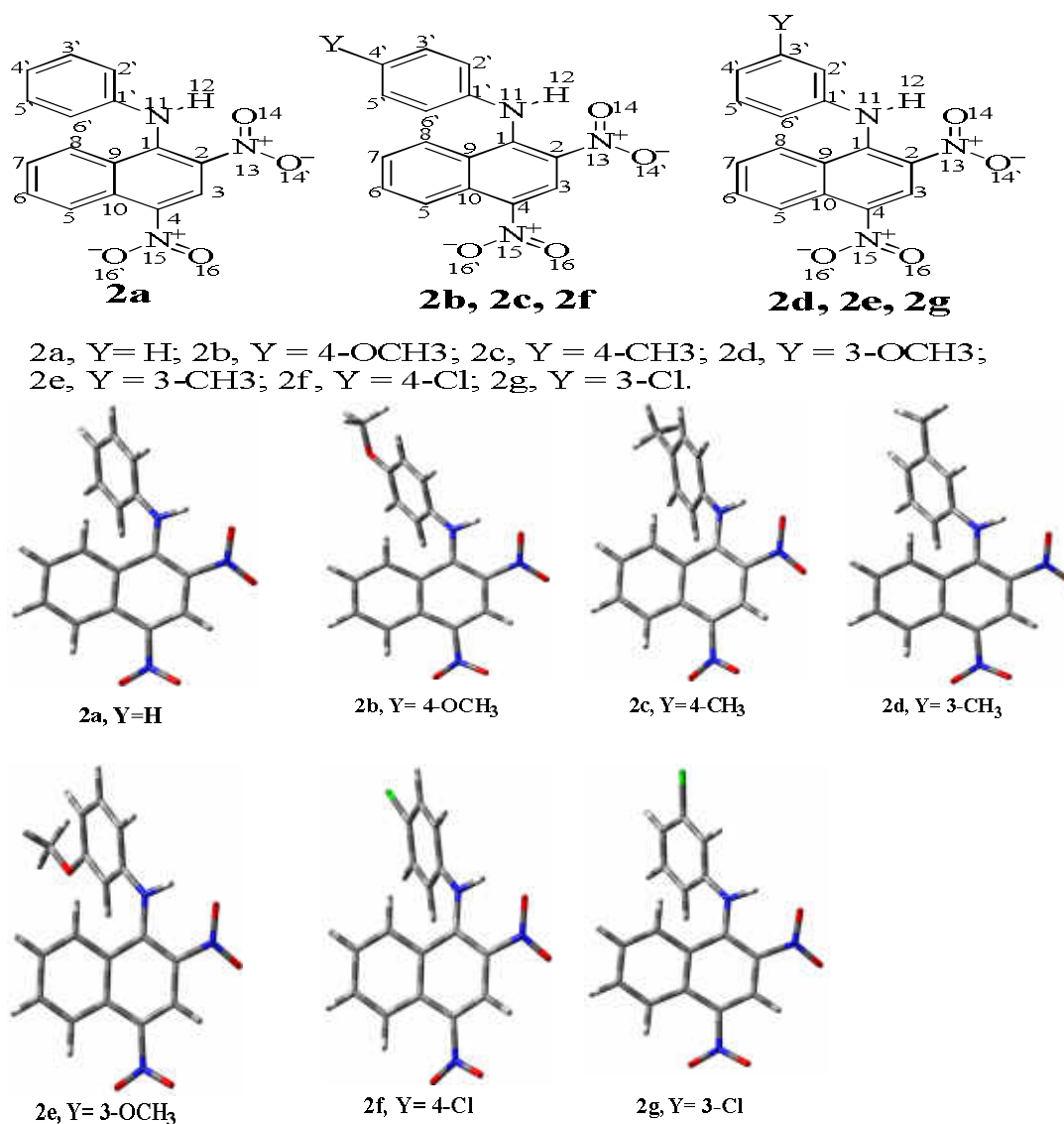


Figure 12. Molecular model of N-aryl 1-(2,4-dinitronaphthyl) amine 2a-g with numbering of atoms.

Table 15. Optimized geometrical parameters (some Bond lengths) of N-Aryl 1-(2,4-dinitronaphthyl) amine 2a-g calculated by B3LYP/6-311G (d, p) density functional calculations

Bond lengths (Å)	Y= H, 2a	Y= 4-OCH ₃ , 2b	Y= 4-CH ₃ , 2c	Y= 3-CH ₃ , 2d	Y= 3-OCH ₃ , 2e	Y= 4-Cl, 2f	Y= 3-Cl, 2g
C ₁ -N ₁₁	1.364	1.359	1.362	1.363	1.363	1.367	1.369
C ₁ -N ₁₃	1.423	1.425	1.424	1.424	1.423	1.422	1.419
C ₂ -N ₁₃	1.459	1.457	1.458	1.459	1.459	1.460	1.461
C ₁ -C ₂	1.413	1.416	1.414	1.413	1.413	1.411	1.410
H ₁₂ -O ₁₄ H-BOND	1.794	1.777	1.787	1.793	1.797	1.795	1.802

The signal for H₆ and H₇ of naphthyl ring appeared as two triplet signals (1H each) in range δ 7.73–8.45 ppm, Figure 3, Table 9. The aryl protons for unsubstituted compound 1a, (X= H) appeared as *ortho* protons H₂ and H₆ showed as doublet at range δ 6.96 ppm, while for *meta* protons H₃ and H₅ exhibited doublet at range δ 7.32 ppm. The *para* proton H₄ showed triplet singlet centered range δ 7.10 ppm. The protons of 4-substituted phenyl 1b, 1c, 1f, 1h resonate at 6.75-6.98 and 7.10-8.24 ppm for H_{2,6'} and H_{3,5'} respectively depending on the nature of substituent. While the protons of 3-substituted phenyl 1d, 1e, 1g resonate at 6.49, 6.92, 7.17 and 6.36-6.75 ppm for H₂, H₄, H₅ and H₆, respectively depending on the nature of substituent. The methyl substituent in compounds 4-methoxy 1b, (X= 4-OCH₃) and 3-methoxy 1e, (X= 3-OCH₃), 4-methyl 1c, (X= 4-CH₃) and 3-methyl 1d, (X= 3-CH₃) showed a singlet (3H) in range δ 2.30 - 3.78 ppm, Table 9. Attempts will be made to study if the H_{2,6'} protons of the aryl ring positioned in the ring current of 2,4-dinitronaphthyl or if H₈ of the naphthyl ring positioned in the ring current of the aryl moiety. This can be reached by applying Hammett correlation between the chemical shift of these protons and σ_{H} constants of substituent which could shed light on the geometry of diaryl ethers 1a-h. However, all these correlations show scattered points indicating that either H₈ or H₂ and H₆ are not positioned in the aryl and naphthyl rings current, respectively. This is consistent with the conformations suggested for ethers 1a-h. The theoretical ¹H NMR chemical shifts of H have been compared with the experimental data as shown in Table 9.

Table 16. Optimized geometrical parameters (some Bond angles) of *N*-aryl 1-(2,4-dinitronaphthyl) amine 2a-g obtained by B3LYP/6-311G (d, p) density functional calculations

Bond angles (°)	Y= H, 2a	Y= 4-OCH ₃ , 2b	Y= 4-CH ₃ , 2c	Y= 3-CH ₃ , 2d	Y= 3-OCH ₃ , 2e	Y= 4-Cl, 2f	Y= 3-Cl, 2g
C ₁ -N ₁₁ -C ₁	128.6°	128.9°	128.8°	128.6°	128.6°	128.4°	128.0°
C ₁ '-N ₁₁ -H ₁₂							
C ₁ -C ₂ -N ₁₃	122.8°	122.9°	122.9°	122.8°	122.8°	122.8°	122.8°
C ₁ -N ₁₁ -H ₁₂	112.1°	111.9°	112.1°	112.1°	112.3°	112.0°	112.1°

Table 17. Optimized geometrical parameters (some dihedral angles) of *N*-aryl 1-(2,4-dinitronaphthyl) amine 2a-g obtained by B3LYP/6-311G (d, p) density functional calculations

Dihedral angles (°)	Y= H, 2a	Y= 4-OCH ₃ , 2b	Y= 4-CH ₃ , 2c	Y= 3-CH ₃ , 2d	Y= 3-OCH ₃ , 2e	Y= 4-Cl, 2f	Y= 3-Cl, 2g
C ₁ '-N ₁₁ -C ₁ -C ₂	142.2°	146.1°	143.9°	142.7°	142.7°	140.8°	139.6°
C ₁ '-N ₁₁ -C ₁ -C ₉	-40.8°	-36.6°	-40.0°	-40.4°	-40.4°	-42.3°	-43.5°
H ₁₂ -N ₁₁ -C ₁ -C ₂	-13.0°	10.9°	-12.1°	-12.8°	-13.1°	-13.5°	14.1°
H ₁₂ -N ₁₁ -C ₁ -C ₉	164.0°	166.5°	164.9°	164.1°	163.8°	163.5°	162.8°
N ₁₁ -C ₁ -C ₂ -N ₁₃	1.3.0°	2.0°	1.6°	1.3°	1.3°	1.2°	0.9°
C ₂ '-C ₁ '-N ₁₁ -C ₁	154.1°	149.5°	152.3°	153.6°	153.7°	156.7°	156.6°
C ₆ '-C ₁ '-N ₁₁ -C ₁	-29.7°	-34.9°	-31.6°	-30.0°	-30.2°	-27.1°	-26.7°

Table 18. Mulliken atomic charges calculated by B3LYP/6-311G (d, p) for *N*-aryl 1-(2,4-dinitronaphthyl) amine 2a-g

Atoms	Y= H 2a	Y= 4-OCH ₃ , 2b	Y= 4-CH ₃ , 2c	Y= 3-CH ₃ , 2d	Y= 3-OCH ₃ , e	Y= 4-Cl, 2f	Y= 3-Cl, 2g
C ₁	0.268	0.269	0.269	0.269	0.271	0.265	0.265
C ₂	0.107	0.108	0.107	0.106	0.105	0.108	0.107
C ₃	0.004	-0.003	0.001	0.003	0.004	0.007	0.009
C ₄	0.098	0.099	0.098	0.098	0.098	0.098	0.097
C ₅	-0.024	-0.025	-0.025	-0.024	-0.024	-0.022	-0.022
C ₆	-0.078	-0.078	-0.078	-0.078	-0.078	-0.077	-0.077
C ₇	-0.082	-0.083	-0.083	-0.083	-0.083	-0.080	-0.080
C ₈	-0.025	-0.026	-0.025	-0.024	-0.022	-0.028	-0.025
C ₉	-0.117	-0.113	-0.116	-0.117	-0.117	-0.119	-0.119
C ₁₀	0.012	0.011	0.012	0.012	0.012	0.014	0.013
C ₁ '	0.053	0.032	0.052	0.062	0.055	0.061	0.058
C ₂ '	-0.046	-0.078	-0.820	-0.073	-0.090	-0.084	-0.028
C ₃ '	-0.087	-0.126	-0.054	-0.093	-0.184	-0.030	-0.236
C ₄ '	-0.090	0.173	-0.103	-0.073	-0.133	-0.244	-0.022
C ₅ '	-0.086	-0.081	-0.070	-0.084	-0.088	-0.030	-0.088
C ₆ '	-0.086	-0.035	-0.041	-0.047	-0.035	-0.045	-0.041
N ₁₁	-0.468	-0.465	-0.468	-0.470	-0.468	-0.471	-0.471
N ₁₃	0.173	0.173	0.173	0.172	0.173	0.173	0.173
N ₁₅	0.146	0.145	0.146	0.146	0.146	0.147	0.147
O ₁₄	-0.322	-0.327	-0.324	-0.323	-0.322	-0.320	-0.318
O ₁₄ '	-0.256	-0.260	-0.258	-0.257	-0.257	-0.253	-0.252
O ₁₆	-0.260	-0.263	-0.261	-0.261	-0.261	-0.258	-0.257
O ₁₆ '	-0.274	-0.276	-0.275	-0.274	-0.274	-0.271	-0.271

The ¹H NMR chemical shifts are calculated within GIAO method applying B3LYP /6-311G(d,p), B3LYP /6-311++G(d,p), BLYP/CC-pVDZ levels. Table 9 shows that there are small differences between the experimental and calculated chemical shift values. This is due to the differences in molecular structure calculation depends on the basis set used as well as the molecular environment.

Molecular orbital analysis of 1a-h: The HOMO and LUMO energies, molecular electrostatic potential (MEP), the global reactivity descriptors(22) and local reactivity descriptors is used to predict the reactivity of 2,4-dinitronaphthyl substituted aryl ether 1a-h.(23) The energy of HOMO characterizes electron donating ability of a molecule while LUMO energy determines the ability to accept an electron. Accordingly, the molecule 1h, (X = 4-NO₂) is considered to be the least molecule has the ability to accept and donates electrons while 1b, (X = 4-OCH₃) has the highest HOMO and LUMO energies that allows it to be the best electron donor and accept molecule, Table 10. The smaller frontier orbital gap is the high chemical stability and low kinetic stability. Table 10 shows that ΔE_{gap} values are arranged in the order 1h, (X= 4-NO₂) > 1g, (X= 3-Cl) > 1a, (X= H) > 1d, (X= 3-CH₃) > 1f, (X= 4-Cl) > 1c, (X= 4-CH₃) > 1e, (X= 3-OCH₃) > 1b, (X= 4-OCH₃). This order indicates that the reactivity of ether derivatives depends on the nature and position of substituents in the aryl moiety.

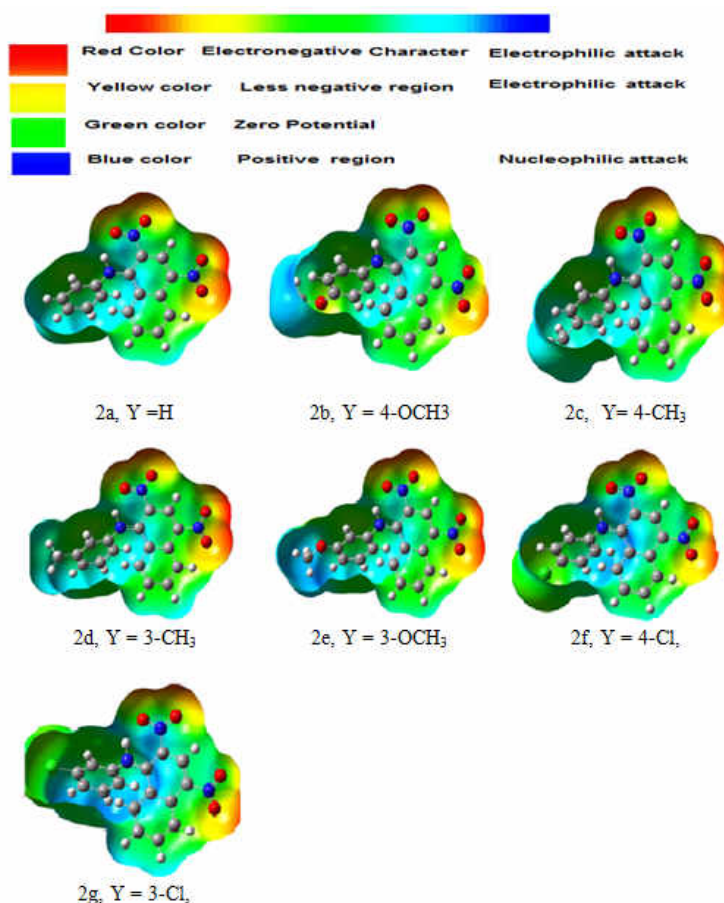


Figure 13. The Molecular Electrostatic Potential (MEP) of *N*-aryl 1-(2,4-dinitronaphthyl) amine 2a-g

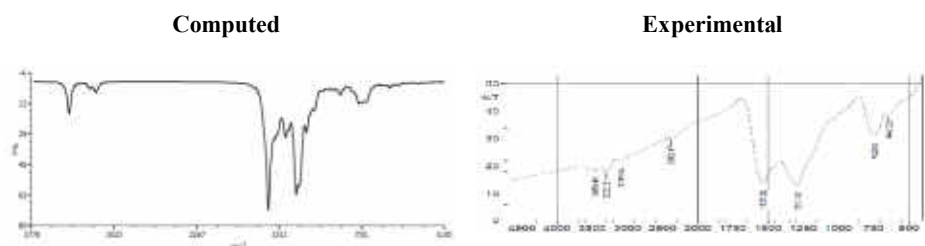
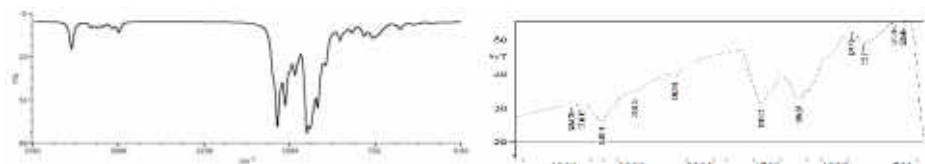
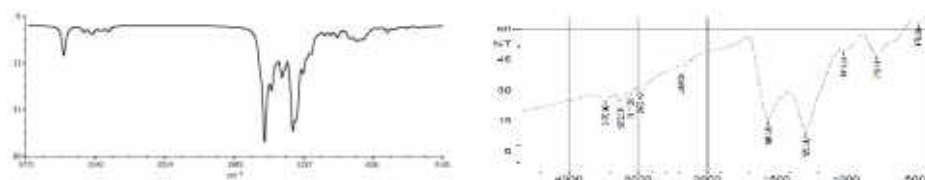
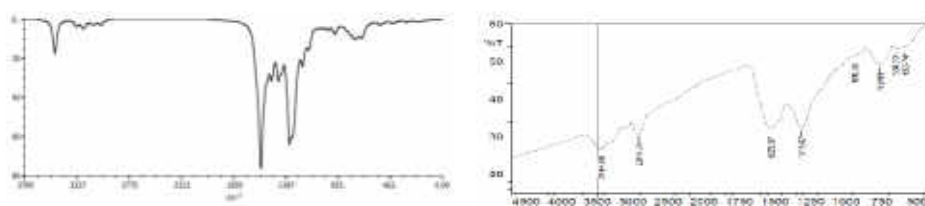
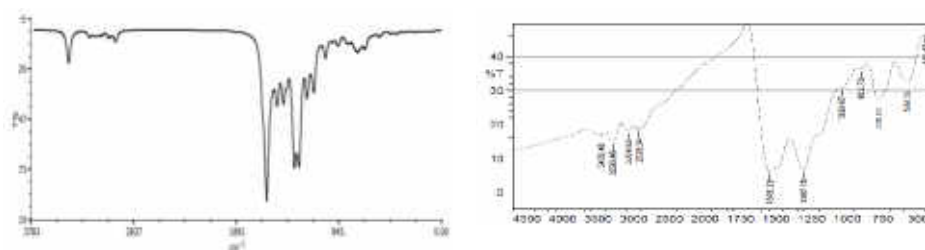
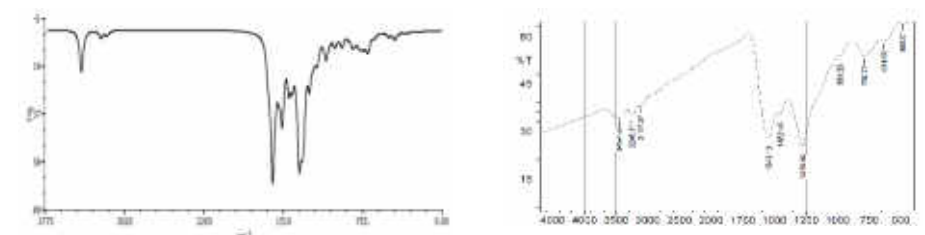
Table 19 Experimental and Calculated B3BLY/6311-G (d, p) level vibrational frequencies (cm^{-1}) of 2a-g.

Cpds	Calculated values					Experimental values		
	$U_{\text{STRECH}} (\text{cm}^{-1})$					$U_{\text{STRECH}} (\text{cm}^{-1})$		
	$\text{N}_{11}\text{-H}_{12}$	$\text{N}_{13}\text{-O}_{14}$	$\text{N}_{13}\text{-O}_{14'}$	$\text{N}_{15}\text{-O}_{16}$	$\text{N}_{15}\text{-O}_{16'}$	$\text{N}_{11}\text{-H}_{12}$	$\text{NO}_2\text{-sym}$	$\text{NO}_2\text{-sym}$
2a	3435	1316	1510	1361	1584	3300	1537	1290
2b	3419	1314	1489	1358	1581	3439	1545	1269
2c	3428	1314	1508	1360	1583	3252	1560	1290
2d	3436	1314	1512	1360	1583	3445	1528	1314
2e	3439	1309	1513	1360	1583	3296	1545	1308
2f	3433	1314	1507	1362	1582	3246	1543	1277
2g	3439	1314	1511	1362	1586	3281	1539	1316

Table 20. The sp^2 C-H stretching vibrations of naphthalene ring in (3a-g)

Cpds	Calculated values										Experimental values
	$v_{\text{STRECH}} (\text{cm}^{-1}), \text{sp}^2\text{-C-H (ArH)}$										$v_{\text{STRECH}} (\text{cm}^{-1})$
	$\text{C}_3\text{-H}_3$	$\text{C}_5\text{-H}_5$	$\text{C}_6\text{-H}_6$	$\text{C}_7\text{-H}_7$	$\text{C}_8\text{-H}_8$	$\text{C}_2\text{-H}_2$	$\text{C}_3\text{-H}_3$	$\text{C}_4\text{-H}_4$	$\text{C}_5\text{-H}_5$	$\text{C}_6\text{-H}_6$	$\text{sp}^2\text{-C-H (ArH)}$
2a	3246	3251	3191	3191	3233	3191	3191	3191	3199	3184	3088
2b	3248	3252	3191	3191	3235	3201	3201	-	3211	3178	2955
2c	3248	3252	3192	3191	3234	3192	3163	-	3183	3183	3111
2d	3246	3251	3191	3191	3233	3198	3198	3181	-	3165	2915
2e	3246	3251	3191	3191	3233	3195	-	3214	3176	3204	3075
2f	3247	3251	3193	3193	3232	3207	3207	-	3207	3182	3117
2g	3245	3250	3192	3192	3232	3202	-	3212	3212	3202	3082

The dipole moment μ (D) is the most widely used quantity to describe the polarity of a covalent bond and measures the net molecular polarity, and it increases with increase in electro negativity of atoms (24). Usually chemical reactivity increases with increase in dipole moment μ (D). Accordingly, our theoretical study suggests that 1b, (X= 4-OCH₃) (μ = 7.15 D) is highest polar molecule whereas 1f, (X= 4-Cl) (μ = 5.35 D) is the lowest one.

**2a, Y=H****2b, Y=4-OCH₃****2c, Y=4-CH₃****2d, Y=3-CH₃****2e, Y=3-OCH₃****2f, Y=4-Cl**

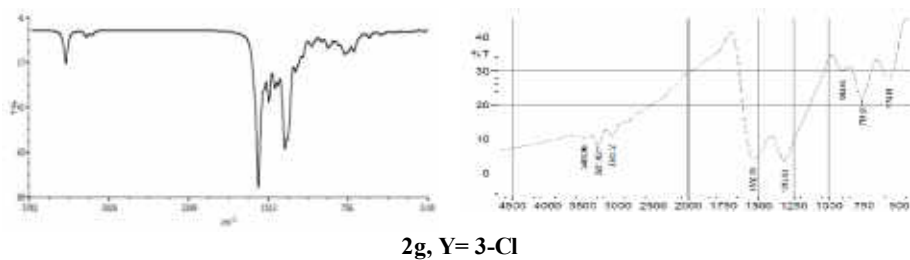
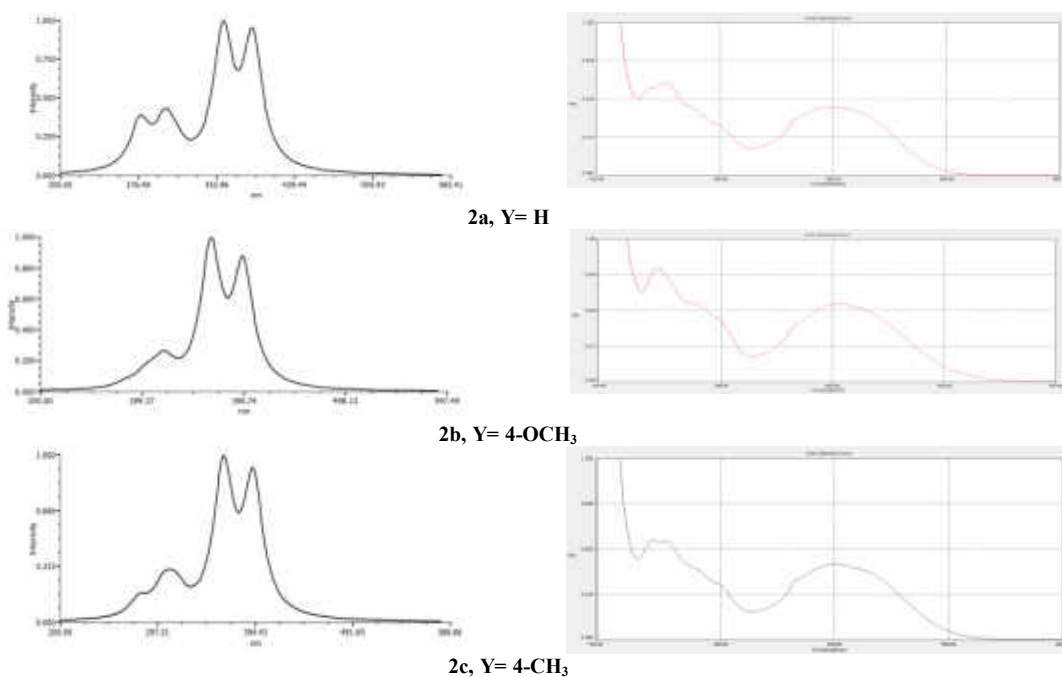


Figure 14. FTIR Spectra of 5a-g, i) Calculated by B3LYP/6-311G (d, p), ii) Experimental.

Table 21. Experimental and Calculated electronic transition properties for amines 2a-g by RTD-CAM-B3LYP-FC/6-311G (d, p) in MSO

Cpds	Experimental λ_{max}	Theoretical λ_{max}	Oscillator strength(f)	Assignment of electronic transition	Electronic transition type
2a, Y=H	400 nm	376 nm	0.310	HOMO-LUMO	$n \rightarrow \pi^*$
	360 nm	342 nm	0.267	HOMO-LUMO+1	$n \rightarrow \pi^*$
	300 nm	296 nm	0.089	HOMO-1-LUMO	$\pi \rightarrow \pi^*$
	275 nm	273 nm	0.063	HOMO-3-LUMO	$\pi \rightarrow \pi^*$
2b, Y= 4-OCH ₃	400 nm	385 nm	0.331	HOMO-LUMO	$n \rightarrow \pi^*$
	360 nm	349 nm	0.311	HOMO-LUMO+1	$n \rightarrow \pi^*$
	310 nm	312 nm	0.049	HOMO-1-LUMO	$\pi \rightarrow \pi^*$
	260 nm	303 nm	0.021	HOMO-5-LUMO	$\pi \rightarrow \pi^*$
2c, Y=4-CH ₃	400 nm	379 nm	0.328	HOMO-LUMO	$n \rightarrow \pi^*$
	360 nm	345 nm	0.289	HOMO-LUMO+1	$n \rightarrow \pi^*$
	300 nm	297 nm	0.057	HOMO-1-LUMO	$\pi \rightarrow \pi^*$
	270 nm	272 nm	0.057	HOMO-3-LUMO	$\pi \rightarrow \pi^*$
2d, Y= 3-CH ₃	400 nm	377 nm	0.317	HOMO-LUMO	$n \rightarrow \pi^*$
	360 nm	343 nm	0.276	HOMO-LUMO+1	$n \rightarrow \pi^*$
	310 nm	297 nm	0.068	HOMO-1-LUMO	$\pi \rightarrow \pi^*$
	260 nm	273 nm	0.055	HOMO-3-LUMO	$\pi \rightarrow \pi^*$
2e, Y=3-OCH ₃	400 nm	374 nm	0.319	HOMO-LUMO	$n \rightarrow \pi^*$
	375 nm	342 nm	0.272	HOMO-LUMO+1	$n \rightarrow \pi^*$
	300 nm	311 nm	0.029	HOMO-1-LUMO	$\pi \rightarrow \pi^*$
	280 nm	278 nm	0.043	HOMO-2-LUMO	$\pi \rightarrow \pi^*$
2f, Y= 4-Cl	400 nm	377 nm	0.351	HOMO-LUMO	$n \rightarrow \pi^*$
	360 nm	340 nm	0.252	HOMO-LUMO	$n \rightarrow \pi^*$
	310 nm	297 nm	0.090	HOMO-1-LUMO	$\pi \rightarrow \pi^*$
	260 nm	273 nm	0.082	HOMO-2-LUMO	$\pi \rightarrow \pi^*$
2g, Y= 3-Cl	390 nm	373 nm	0.329	HOMO-LUMO	$n \rightarrow \pi^*$
	310 nm	338 nm	0.237	HOMO-LUMO+1	$n \rightarrow \pi^*$
	300 nm	296 nm	0.112	HOMO-1-LUMO	$\pi \rightarrow \pi^*$
	270 nm	273 nm	0.076	HOMO-3-LUMO	$\pi \rightarrow \pi^*$



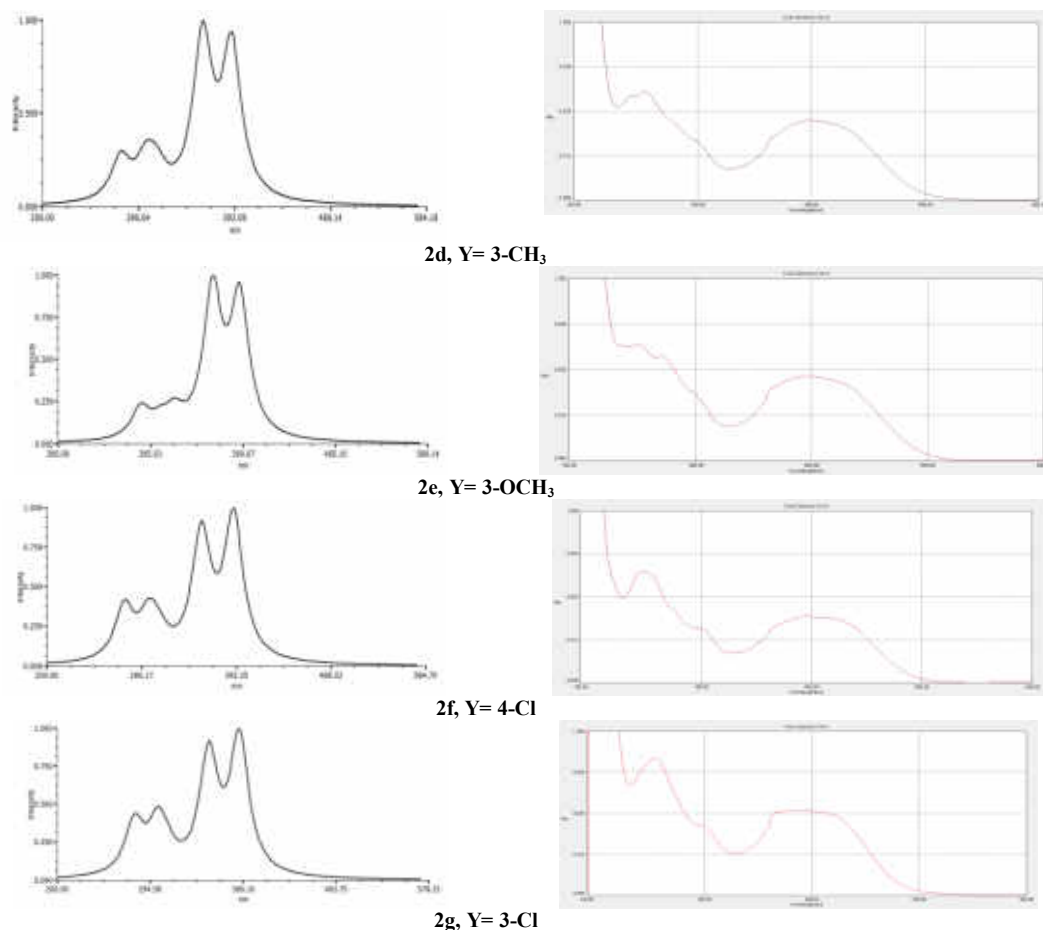


Figure 15 Computed and Experimental UV-VIS absorption spectra of amines 2a-g

Table 22. Calculated Energies and related molecular properties values of *N*-aryl 1-(2,4-dinitronaphthyl) amine 2a-g by B3LYP/6-311G (d, p)

descriptor	2a	2b	2c	2d	2e	2f	2g
E_{HOMO}	-6.46	-6.17	-6.36	-6.41	-6.39	-6.56	-6.64
E_{LUMO}	-3.03	-2.91	-2.97	-2.99	-2.97	-3.18	-3.19
ΔE_e	3.43	3.26	3.38	3.42	3.42	3.38	3.46
I_p	6.46	6.17	6.36	6.41	6.39	6.56	6.64
E_A	3.03	2.91	2.97	2.99	2.97	3.18	3.19
\square (D)	7.58	9.32	8.22	8.02	9.05	5.72	5.96
\square	4.75	4.54	4.67	4.70	4.68	4.87	4.92
\square (eV)	-4.75	-4.54	-4.67	-4.70	-4.68	-4.87	-4.92
η	1.71	1.63	1.69	1.71	1.71	1.69	1.73
S	0.58	0.61	0.59	0.59	0.58	0.59	0.58
ω	6.57	6.32	6.43	6.47	6.39	7.01	7.00

Table 23. Optimized geometrical parameters of 1-naphthyl piperidine6 obtained by B3LYP/6-311G density functional calculations

Bond Length (Å)	B3LYP/6-311 G(d,p)	Bond angles (°)	B3LYP/6-311 G(d,p)	Dihedral angles (°)	B3LYP/ 6-311 G(d,p)
C_1-N_{11}	1.434	$C_2-N_{11}-C_1$	117.5°	$C_2-N_{11}-C_1-C_2$	108.6°
C_2-N_{11}	1.464	$C_6-N_{11}-C_1$	117.5°	$C_2-N_{11}-C_1-C_9$	-71.4°
C_6-N_{11}	1.464	$N_{11}-C_1-C_2$	117.2°	$C_6-N_{11}-C_1-C_2$	108.6°
C_1-C_2	1.397	$N_{11}-C_1-C_9$	123.6°	$C_6-N_{11}-C_1-C_9$	-71.4°
C_1-C_9	1.435				

Molecular Electrostatic Potential (MEP) of 1a-h: The chemical reactivity of a compound is easily determined with the help of MEP surface analysis which differentiate the electrophilic and nucleophilic sites in a molecule quite easily. The MEP (25) maps of 1a-h show that the negative potential sites are on electronegative oxygen atoms represented by red color and the blue color related to the positive potential sites are around the hydrogen atoms attached to naphthalene ring and all atoms of aryl ring. Whereas, zero potential represented by the green color disperses on all carbon atoms of the naphthalene ring, Figure 8. These sites give information about the region from where the compounds 1a-h can have intermolecular interactions and predicted the most reactive site for both electrophilic and nucleophilic attack. Intensive view of Figure 8 reveals that most C_{11} atoms located in the blue color region while most C_1 atoms locate in the green color region. Accordingly, the predicted most reactive site for nucleophilic attack is C_{11} while C_1 atom is susceptible for both nucleophilic and electrophilic attack.

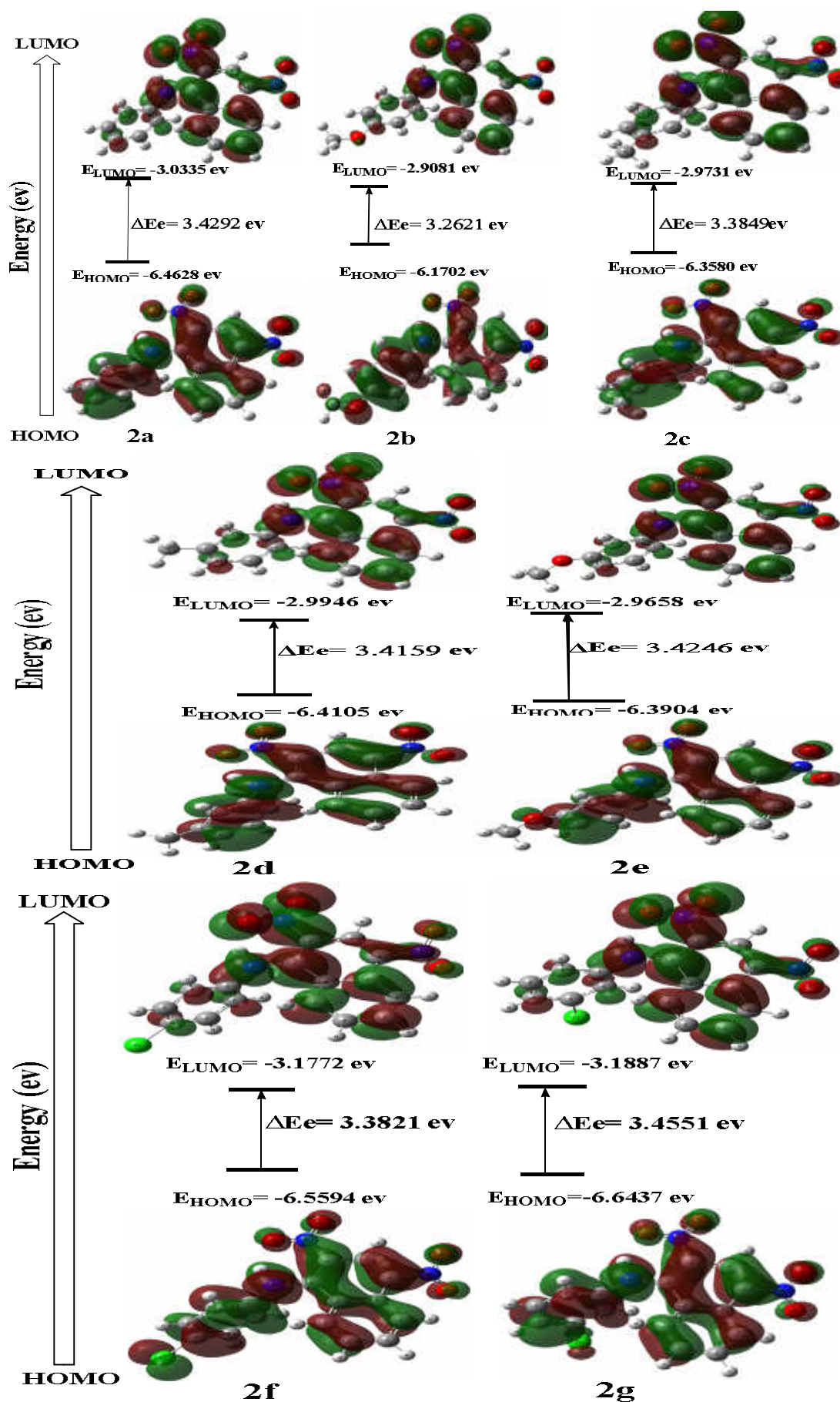
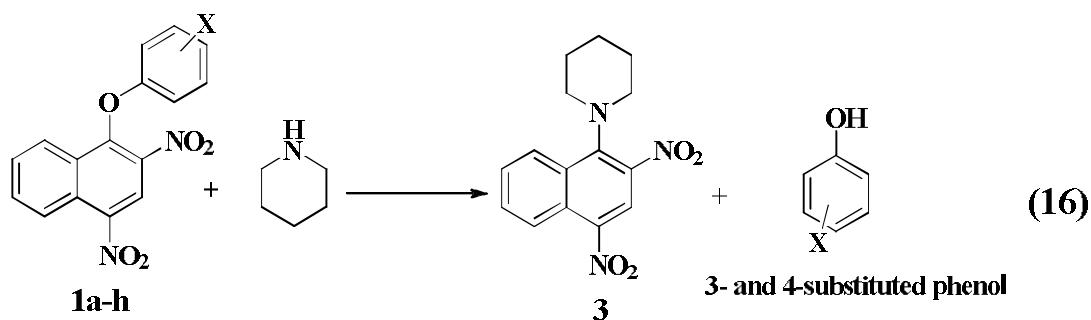


Figure 16. HOMO and LUMO Energy gap diagram of 2a-g.



(a, X = H; b, X = 4-OCH₃; c, X = 4-CH₃; d, X = 3-CH₃; e, X = 3-OCH₃; f, X = 4-Cl; g, X = 3-Cl; h, X = 4-NO₂)

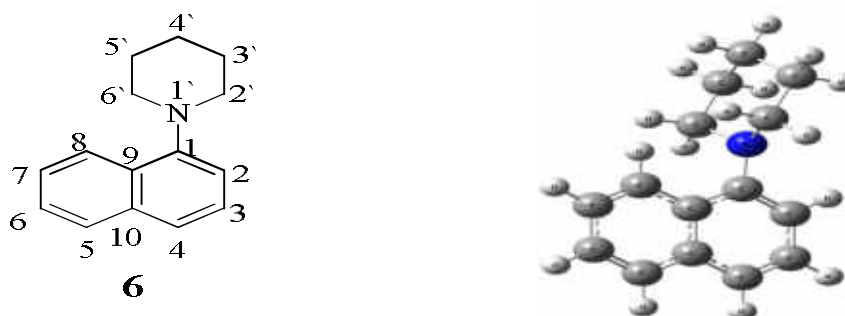


Figure 17. Molecular modeling of 1-naphthyl piperidine 6 with numbering of atoms.

Table 24. The Mulliken charge distribution of 1-naphthyl piperidine 6 obtained by B3LYP/6-311G (d, p) density functional calculations.

Atoms	Mulliken	Atoms	Mulliken
H ₂	0.086	C ₁	0.020
H ₃	0.092	C ₂	-0.021
H ₄	0.080	C ₃	-0.098
H ₅	0.083	C ₄	-0.041
H ₆	0.092	C ₅	-0.064
H ₇	0.089	C ₆	-0.085
H ₈	0.100	C ₇	-0.101
H _{2'}	0.114	C ₈	-0.062
H _{3'}	0.084	C ₉	-0.020
H _{4'}	0.105	C ₁₀	-0.057
H _{5'}	0.106	C _{2'}	-0.043
H _{6'}	0.113	C _{3'}	-0.190
H _{7'}	0.099	C _{4'}	-0.242
H _{8'}	0.105	C _{5'}	-0.190
H _{9'}	0.106	C _{6'}	-0.043
H _{10'}	0.114		
H _{11'}	0.084		
N _{1'}	-0.457		

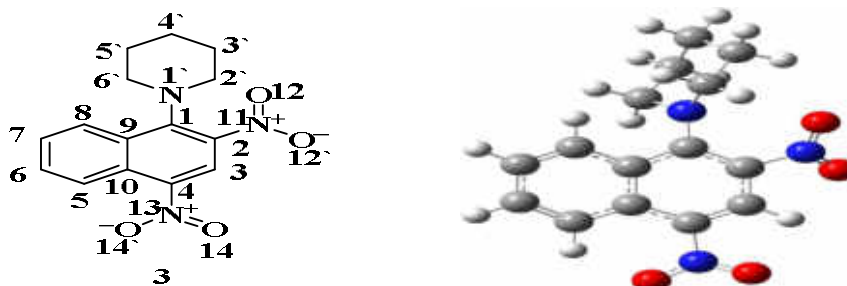


Figure 18. Molecular modeling of 1-(2,4-dinitrophenyl)piperidine 3 with numbering of atoms

Global reactivity descriptors of 1a-h: The global chemical reactivity descriptors were obtained at the level of theory B3LYP/6-311G (d, p) and are calculated from HOMO and LUMO energies, Table 10. They are namely (26-30), ionization potential (I_p), electron affinity (E_A), chemical potential ($\mu = -\chi$), the absolute electro negativity (χ) is given by the relation ($\chi = (I_p + E_A)/2$),

Table 25. Optimized geometrical parameters of 1-(2,4-dinitronaphthalen-1-yl) piperidine 3 obtained by B3LYP/6-311G (d, p) density functional calculations

Bond Length (Å)	B3LYP/6-311 G(d,p)	Bond angles(°)	B3LYP/6-311 G(d,p)	Dihedral angles (°)	B3LYP/ 6-311 G(d,p)
C ₁ -N ₁₁	1.403	C ₁ N ₁₁ C ₂₁	120.5°	C ₂ N ₁₁ -C ₁ C ₂	-84.1°
C ₁ -C ₂	1.395	C ₁ N ₁₁ C ₆	120.1°	C ₆ N ₁₁ -C ₁ C ₉	-56.4°
C ₁ -C ₉	1.444	N ₁₁ C ₁ C ₂	121.7°	C ₂ N ₁₁ -C ₁ C ₉	98.9°
		N ₁₁ C ₁ C ₉	121.7°	C ₆ N ₁₁ -C ₁ C ₂	120.5°
		C ₁ C ₂ N ₁₁	122.4°		

Table 26. Mulliken, NBO atomic charge for 1-(2,4-dinitronaphthalen-1-yl) piperidine 3.

Atomic charge	Mullikencharge	NBO charge
H ₃	0.159	0.264
H ₅	0.126	0.263
H ₆	0.109	0.209
H ₇	0.102	0.208
H ₈	0.116	0.212
H ₂	0.101	0.159
H ₂₁	0.135	0.219
H ₃₁	0.110	0.200
H ₃₁	0.135	0.209
H ₄₁	0.099	0.181
H ₄₁	0.120	0.202
H ₅₁	0.113	0.200
H ₅₁	0.115	0.195
H ₆₁	0.091	0.157
H ₆₁	0.127	0.203
C ₁	0.191	0.256
C ₂	0.121	0.058
C ₃	0.056	-0.165
C ₄	0.093	0.088
C ₅	-0.017	-0.177
C ₆	-0.078	-0.166
C ₇	-0.086	-0.186
C ₈	-0.049	-0.170
C ₉	-0.062	-0.061
C ₁₀	0.009	-0.046
C ₂₁	-0.052	-0.159
C ₃₁	-0.189	-0.383
C ₄₁	-0.247	-0.377
C ₅₁	-0.184	-0.375
C ₆₁	-0.060	-0.164
N ₁₁	-0.479	-0.537
N ₁₁	0.163	0.52
N ₁₃	0.146	0.515
O ₁₂	-0.256	-0.382
O ₁₂	-0.259	-0.377
O ₁₃	-0.253	-0.375
O ₁₃	-0.265	-0.388

Table 27. Calculated B3BLY/6-311G (d, p) level vibrational frequencies (cm⁻¹) 1-(2,4-dinitronaphthalen-1-yl)piperidine3

Cpd	Calculated values						
	ν _{TRECH} (cm ⁻¹)						
3	C ₁ -N ₁₁	N ₁₁ -O ₁₂	N ₁₁ -O ₁₂	N ₁₃ -O ₁₄	N ₁₃ -O ₁₄	C ₂ -N ₁₁	C ₄ -N ₁₃
	1430	1622	1377	1641	1361	942(331)	1000(395)

Table 28 Calculated B3BLY/6311-G (d, p) level vibrational frequencies (cm⁻¹) of the sp² C-H and sp³ C-H stretching vibrations of 1-(2,4-dinitronaphthalen-1-yl)piperidine3.

Cpd	ν _{TRECH} (cm ⁻¹), sp ² C-H				
	C ₃ -H ₃	C ₅ -H ₅	C ₆ -H ₆	C ₇ -H ₇	C ₈ -H ₈
3	3239	3250	3191	3191	3241
	ν _{TRECH} (cm ⁻¹), sp ³ C-H (piperidine)				
	C ₂ -H ₂	C ₂ -H ₂	C ₃ -H ₃	C ₃ -H ₃	C ₄ -H ₄
	2921	3125	3086	3088	3061
	C ₄ -H ₄	C ₅ -H ₅	C ₅ -H ₅	C ₆ -H ₆	C ₆ -H ₆
	3001	3070	3070	2941	3088

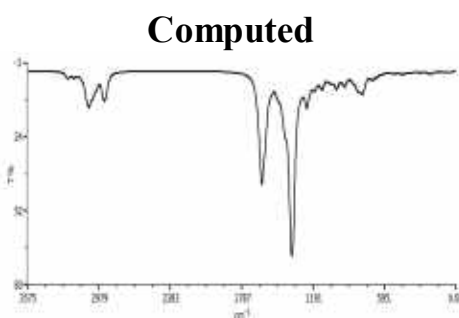


Figure 19. FTIR Spectra of 1-(2,4-dinitronaphthalen-1-yl) piperidine 3 Calculated by B3LYP/6-311G (d, p).

Table 29. Experimental and calculated of electronic transition properties for 1-(2,4-dinitronaphthalen-1-yl) piperidine 8 in DMSO

Methods	Experimental λ_{\max}	Theoretical λ_{\max}	Oscillator strength (<i>f</i>)	Assignment of electronic transition	Electronic transition type
TD-DFT/ CAM-B3LYP/ 6-311++G (d,p)		419	0.117	HOMO-LUMO	$n \rightarrow \pi^*$
		350	0.161	HOMO-LUMO+1	$n \rightarrow \pi^*$
		325	0.076	HOMO-1-LUMO	$\pi \rightarrow \pi^*$
		288	0.030	HOMO-1-LUMO+1	$\pi \rightarrow \pi^*$
TD-DFT/ CAM-B3LYP/ 6-311G (d,p)	420 400 360 280	405	0.115	HOMO-LUMO	$n \rightarrow \pi^*$
		355	0.142	HOMO-LUMO+1	$n \rightarrow \pi^*$
		317	0.065	HOMO-1-LUMO	$\pi \rightarrow \pi^*$
		280	0.044	HOMO-2-LUMO	$\pi \rightarrow \pi^*$
TD-DFT/ B3LYP/ 6-311G (d,p)		494	0.098	HOMO-LUMO	$n \rightarrow \pi^*$
		432	0.054	HOMO-LUMO+1	$n \rightarrow \pi^*$
		370	0.078	HOMO-1-LUMO	$\pi \rightarrow \pi^*$
		326	0.082	HOMO-2-LUMO	$\pi \rightarrow \pi^*$

Figure 20. Computed and Experimental UV-VIS absorption spectrums of 1-(2,4-dinitronaphthalen-1-yl) piperidine 3

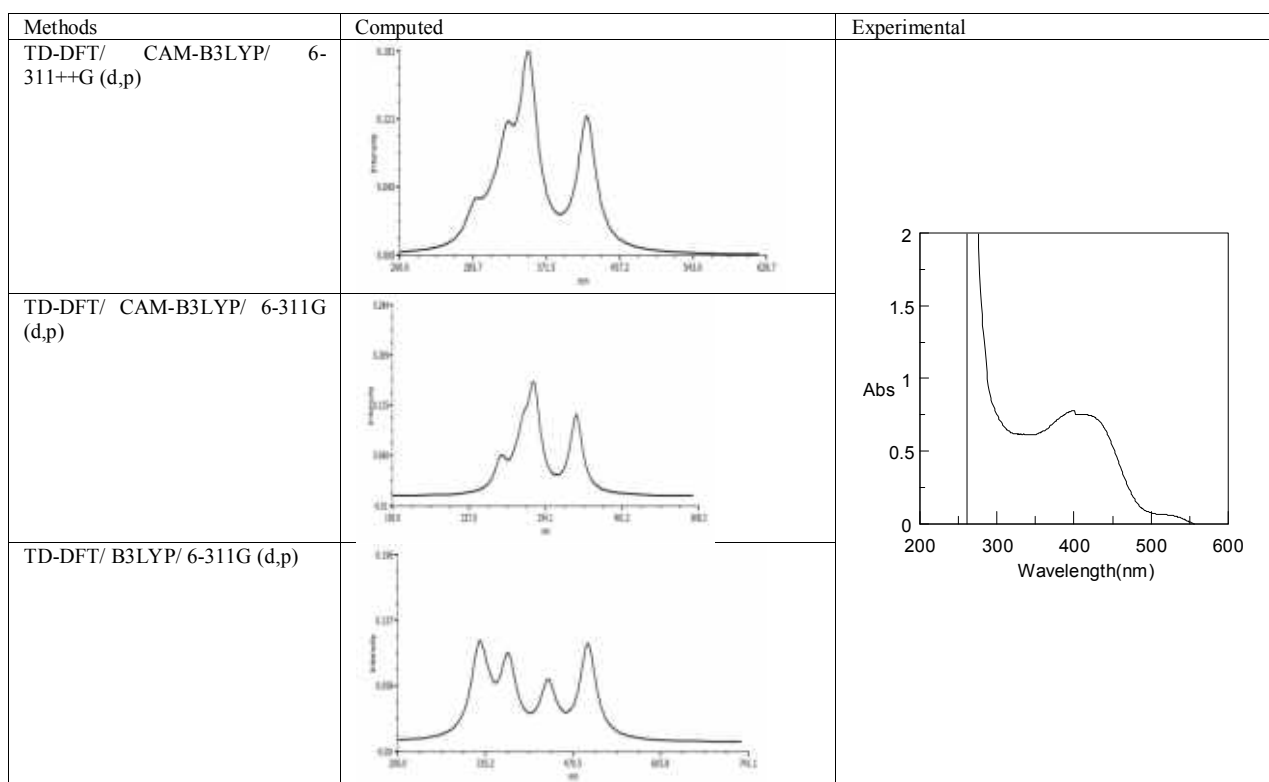
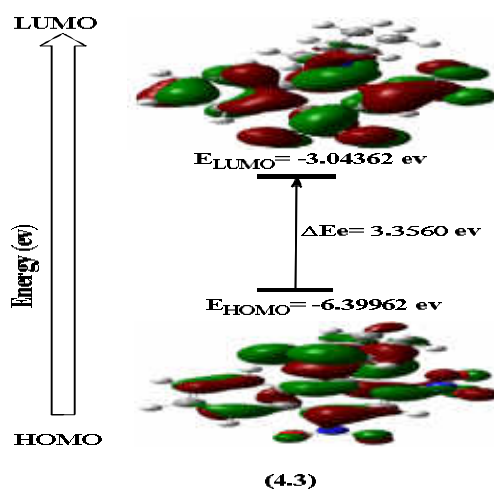
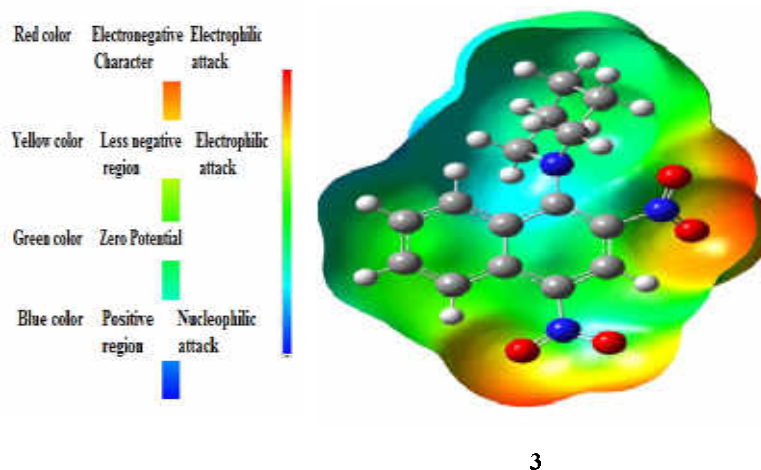


Table 30. Theoretical ^1H chemical shift (ppm) of 1-(2,4-dinitronaphthalen-1-yl) piperidine 3

Proton	H ₃	H ₅	H ₆	H ₇	H ₈	H _{2'}	H _{2''}	H _{3'}	H _{3''}	H _{4'}	H _{4''}	H _{5'}	H _{5''}	H _{6'}	H _{6''}
B3LYP/6-311g (d, p)	9.56	9.93	8.77	8.62	9.11	4.10	4.44	2.34	2.82	2.51	2.19	2.25	2.10	4.40	3.53
BLYP/6-311g (d, p)	9.39	9.94	8.75	8.63	9.18	4.51	4.811	2.729	3.07	2.92	2.56	2.68	2.44	4.90	3.99

Table 31 Calculated Energies and related molecular properties values of 1-(2,4-dinitronaphthalen-1-yl) piperidine 3 by B3LYP/6-311G (d, p)

Cpd	E_{HOMO}	E_{LUMO}	ΔE_e	I_p	E_A	χ	χ	η	S	ω	$\Delta\chi_{\text{min}}$	Nu index
3	-6.40	-3.04	3.36	6.40	3.04	4.72	-4.72	3.36	0.30	3.32	1.41	2.97

**Figure 22.** HOMO and LUMO Energy Gap diagram of 1-(2,4-dinitronaphthalen-1-yl) piperidine 3.**Figure 23.** The Total Electron Density surface mapped with Electrostatic Potential of 3.

global hardness (η) and global softness (S) are defined as ($\eta = (E_{LUMO} - E_{HOMO})/2$) and ($S = 1/2\eta$) respectively, and the electrophilicity (ω) can be calculated using the electronic chemical potential and the chemical hardness ($\omega = \mu^2/2\eta$).

Ionization potential (I_p): It is the amount of energy needed to remove an electron from its atom, molecule, or radical i.e. electron donor (31) shown by Equation (2). High ionization energy indicates high stability. Table 10 shows that the better electron

$$I_p = -E_{HOMO} \quad (2)$$

donor and the more stable molecule are 1h, ($X = 4\text{-NO}_2$) while the lowest electron donor and the least stable molecule is 1b, ($X = 4\text{-OCH}_3$). The electron donor follows the order 1h, ($X = 4\text{-NO}_2$) > 1g, ($X = 3\text{-Cl}$) > 1f, ($X = 4\text{-Cl}$) > 1a, ($X = \text{H}$) ~ 1d, ($X = 3\text{-CH}_3$) > 1c, ($X = 4\text{-CH}_3$) > 1e, ($X = 3\text{-OCH}_3$) > 1b, ($X = 4\text{-OCH}_3$).

The electron affinity (E_A): It is the energy released when an electron is added to a neutral molecule i.e. electron acceptor (32). Because LUMO orbital can accept electrons and responsible for reactivity of nucleophilic reaction, therefore its energy is directly related to electron affinity (E_A), Equation (3). Table 10 reveals that 1h, ($X = 4\text{-NO}_2$) is the highest molecule whereas 1b, ($X = 4\text{-OCH}_3$) molecule is the lowest one that can form negative ion.

$$E_A = -E_{LUMO} \quad (3)$$

The electron acceptor to LUMO orbital follows the order: 1h, (X= 4-NO₂) > 1f, (X= 4-Cl) > 1g, (X= 3-Cl) > 1a, (X= H) > 1c, (X= 4-CH₃) ~ 1d, (X= 3-CH₃) > 1e, (X= 3-OCH₃) > 1b, (X= 4-OCH₃). This is the expected order of reactivity of 1a-h with nucleophiles.

Chemical potential (μ): The chemical potential μ (eV) measures the escaping tendency of an electron(33) and it can be associated with the molecular electronegativity. The values of μ were calculated by Equation (4) and for all compounds are presented in Table 10.

$$\mu \approx -\frac{1}{2}(I_P + E_A) \approx \frac{1}{2}(E_{LUMO} - E_{HOMO}) \quad (4)$$

From the Table 10, the ether contains 4-methoxyphenyl moiety is less stable and more reactive in the gas phase and 4-nitrophenyl moiety is more stable and less reactive. The order of stability of compounds 1a-h is: 1h, (X= 4-NO₂) > 1g, (X= 3-Cl) > 1f, (X= 4-Cl) > 1a, (X= H) > 1d, (X= 3-CH₃) > 1c, (X= 4-CH₃) > 1e, (X= 3-OCH₃) > 1b, (X= 4-OCH₃).

Electronegativity (χ): The concept of electronegativity (χ) was first introduced by Pauling (34) which represents the “power” of an atom in a molecule to attract the bonded electrons towards it. Later, Mulliken (35) described (χ) as the average of the first ionization potential (I_P) and the electron affinity (E_A). He showed that (χ) could be determined by an arithmetic mean of the corresponding (I_P) and (E_A) values as given in Equation (5).

$$\chi = \frac{E_A + I_P}{2} \quad (5)$$

The best electron acceptor of 1a-h is directly proportional to electro negativity value (χ). Table 10 shows that this parameter follows the order: 1b, (X= 4-OCH₃) < 1e, (X= 3-OCH₃) < 1c, (X= 4-CH₃) < 1d, (X= 3-CH₃) < 1a, (X= H) < 1f, (X= 4-Cl) < 1g, (X= 3-Cl) < 1h, (X= 4-NO₂). i.e. the best electron acceptor is 1h, (X= 4-NO₂) and the least one is 1b, (X= 4-OCH₃). This is the same order observed for the calculated (I_P) parameters’

Chemical hardness (η) and softness (S): It has been reported that the behavior of chemical reaction of compounds understood from their hardness (η) and softness (S) values. Hard nucleophiles have a low energy HOMO, a high energy LUMO and a large energy gap. Whereas, soft nucleophiles have a high energy HOMO, a low energy LUMO and a small energy gap(36).

Chemical hardness (η): Chemical hardness (η) measures the resistance of an atom to charge distribution in a molecule(37). It was calculated by using of Equation (6) and is presented in Table 10. It showed that similar trend of 1a-h to the ΔE_{gap} , because of the chemical hardness (η) is equal to the energy gap difference between the LUMO and HOMO orbitals. The larger the HOMO-LUMO energy gaps the harder molecule. Table 10 shows that the greater hardness of 1h, (X= 4-NO₂) makes it the most stable compound while the lower hardness value of 1b, (X= 4-OCH₃) causes it the least stable one.

Theoretical calculations established that the molecule 1h, (X= 4-NO₂) has the highest hardness value ($\eta = 1.98$ eV), indicating that it is the hardest molecule and makes it the most stable compound in the series 1a-h while the lower hardness value of 1b, (X= 4-OCH₃) has the least hardness and causes it the least stable one. Chemical softness (S): Global softness (S) describes the capacity of an atom or group of atoms to receive electrons(31). i.e. has the ability to disperse or delocalize electrons. The reciprocal of (η) and hence represents the extent to which the electronic environment surrounding the nucleus/nuclei of an atomic/molecular species tends to loosen itself. It is expressed in Equation (7), (8):

$$S = \frac{1}{\eta} \quad (7)$$

$$S = \frac{1}{\eta} \cong -2 / (E_{HOMO} - E_{LUMO}) \quad (8)$$

The soft molecules will be more polarizable than hard molecules. Inversely to the value of hardness (η), the compound 1b, (X= 4-OCH₃) has the highest softness (S = 0.67 eV) in the same series 1a-h, so it is the softest compound.

Electrophilicity index (ω): The concept of electrophilicity viewed as a reactivity index(33). The electrophilicity is a descriptor of reactivity that allows a quantitative classification of the global electrophilic nature of a molecule within a relative scale (29) It is defined by the electronic chemical potential (μ) and the chemical hardness (η)(29) shown by Equation (9).

$$\omega = \frac{\mu^2}{2\eta} \quad (9)$$

A good reactive electrophile is characterized by a high value of (ω). Thus, the electrophilicity of ether derivatives 1a-h are arranged in following order: 1h, (X= 4-NO₂) > 1g, (X= 3-Cl) > 1a, (X= H) > 1d, (X= 3-CH₃) > 1f, (X= 4-Cl) > 1c, (X= 4-CH₃) > 1e, (X= 3-OCH₃) > 1b, (X= 4-OCH₃), Table 10. It is observed from this order one suggests that ether contains 4-chlorophenyl moiety is less electrophilic than phenyl itself because 1f, (X= 4-Cl) substituent donates electron to center of reaction by mesomeric effect which overcome its electron withdrawing by inductive like 1b, (X= 4-OCH₃) and in turn decreases the electrophilicity and in turn inhibits

the possible nucleophilic attack. Attempts are made to correlate the calculated global reactivity descriptors against σ -Hammett constants (Fig. not shown). These plots show poor correlations and σ -Hammett values are directly proportional with positive slope for ΔE_{gap} , I_p , χ and η , whereas a negative slope was observed for μ and S , the relation of Hammett values and with (ω) showed scattered correlations. These plots point out that the global parameters are poorly depend on the polar effect of substituent in the aryl moiety and their resonance effect play pronounced factor.

Local Reactivity Descriptors: The Fukui functions correspond to the site k of a molecule while f_k values Equations (10) are indicators that are used to identify the most favored nucleophile-electrophile attacks. The local version of the electrophilicity index has been proposed by employing a resolution of identity as follows (35).

$$\omega_k^\alpha \text{ or } f_k^\alpha \quad (10)$$

Where f_k is the Fukui function at atom k in a molecule and ($\alpha = +, -$ and 0) represents local philic quantities describing nucleophilic, electrophilic and radical attacks respectively. Fukui functions $f^+(r)$, $f^-(r)$ and $f^0(r)$ are calculated using the following Equations (11, 12 and 13) as: (35)

$$f^+ = (q(N+1) - q(N)), \text{ for nucleophilic attack, (acts as a nucleophile).} \quad (11)$$

$$f^- = (q(N) - q(N-1)), \text{ for electrophilic attack, (acts as an electrophile).} \quad (12)$$

$$f^0 = (q(N+1) - q(N-1))/2, \text{ for radical attack.} \quad (13)$$

Where q_k is atomic charge at the k^{th} atomic site in the anionic ($N+1$), cationic ($N-1$) or neutral molecule. Parr and Yang showed that sites in chemical species with the largest values of Fukui function (f_k) shows high reactivity for corresponding attacks. In the title compounds 1a-h, the order of the reactive sites for electrophilic attack, nucleophilic attack and free radical attacks is given in Tables 11. The competition between the electrophilic centers in compounds contain more than one center have been reported with a variety of nucleophiles (38). The choice between two electrophilic centers depends on (i) the structure of the compound under nucleophilic attack (ii) the nature of reagent (iii) the basicity of the leaving group from the reactant compared to that of the attacking nucleophile, (iv) the nature of substituent in the non-leaving or leaving group containing the reactant, (v) the stability of activated complex formed in the rate limiting step, (iv) Application of Klopman equation to investigate the relative reactivity of the two electrophilic centers namely ($C_1, C_{1'}$) toward nucleophilic attack (39) and (iv) the relative "hardness" and "softness" of the reaction site and reagent. In fact the choice between two electrophilic centers is mainly depending on the stability of the activated complex formed in the slow step due to nucleophilic attack at a given electrophilic center. Since the stability-reactivity of activated complexes cannot determine easily, authors use quantum chemistry to determine the reactivity order of closely related reagents or reactants toward a given reaction center, and predicting the properties of the activated complex. Other important factor is the basicity of the leaving groups split from series of reactants compared to those of the attacking nucleophiles or *vice versa*. Since, phenyl and naphthyl rings in compounds 1a-h are not planar and may reduce the ability of fast attack by nucleophiles from the front side, the nucleophilic attack on C_1 and $C_{1'}$ can interact by a same manner. Such attack on the ipso carbon of aryl ring $C_{1'}$ is likely predominated and 2,4-dinitronaphthoxide ion may possible the leaving group. The Mulliken, NBO charges and atomic orbital coefficient of LUMO show that the naphthyl ipso carbon (C_1) is more positively charged atom than the aryl ipso carbon ($C_{1'}$). This indicates that the interaction of a nucleophile with the naphthyl ipso carbon C_1 is controlled by its charge, while the reaction of the nucleophile with the aryl ipso carbon $C_{1'}$ would be controlled by its coefficient (39). Thus $C_{1'}$ can be considered as higher hard (less softness) electrophilic center while C_1 is less hard (higher softness) one. As a result, one can suggest that the regioselectivity of the nucleophilic reaction depends on the nature of the attacking nucleophile. MEP predicts that the most reactive site for nucleophilic attack is $C_{1'}$ while C_1 atom is susceptible for both nucleophilic and electrophilic attacks. An alternative concept, the regioselectivity of nucleophilic attack on ether 1a-h is presumably achieved from the ability of the possible leaving group attached to $C_{1'}$ or C_1 if phenoxide anion or 2,4-dinitronaphthoxide anion having pK_a values 9.81 and 2.12 respectively. These pK_a values of both leaving groups indicate 2,4-dinitro-naphthoxide as leaving group predominates and the nucleophile chooses attack on $C_{1'}$. Further concept is directed to compare the stability of the activated complexes formed in the slow step due to attack on C_1 or $C_{1'}$. As a result, the authors have concluded that the regioselectivity of the nucleophilic reaction on the titled ethers 1a-h depends on the softness (hardness) of the attacking nucleophile.

Accordingly, we suggest that, the regioselectivity of nucleophilic attack on ether 1a is presumably achieved from calculating and comparing the energies of the activated complexes obtained from such attack on C_1 and $C_{1'}$. It was well known that Meisenheimer intermediates III-1 or III-2 are the possible intermediates for reaction of ether 1a with charged nucleophile such as hydroxide ion on C_1 or $C_{1'}$ respectively. While, the zwitterion intermediates II-1 or II-2 are formed in the first step of uncatalyzed nucleophilic aromatic substitution reaction using amine as nucleophile such as aniline on C_1 or $C_{1'}$ respectively. Whereas, the proton transfer process leading to II intermediate is the rate controlling step for such catalyzed reaction. Table 12 indicates that the stability of II or III formed due to uncatalyzed attack of aniline or hydroxide ion on C_1 is higher than obtained from attack of these nucleophiles on $C_{1'}$. Also, III intermediate obtained from catalyzed reaction of aniline with C_1 is more stable than this obtained from nucleophilic attack on $C_{1'}$. Accordingly, the regioselectivity of nucleophilic attack on ether 1a-h is predominating on C_1 rather than $C_{1'}$.

The perturbation theory is one of the fundamental theories in organic chemistry and describes chemical reactivity in terms of frontier orbitals and the charge of the molecules. (40) In fact, most reactions are dominated by either frontier orbital interactions or

charge interactions as described in the simplified Klopman equation, with the first term denoting the contribution of the charge and the second term denoting the contribution of the orbital interaction. Klopman equation is studied in the present work in order to investigate the relative reactivity of the two electrophilic centers namely (C_1 , $C_{1'}$) toward nucleophilic attack. The simplified form of Klopman equation is given below in **Equation (14)**.(41).

$$\Delta E = \underbrace{-\frac{Q_{nuc}Q_{elec}}{\epsilon R}}_{\text{Electrostatic Term}} + 2 \underbrace{\frac{(C_{nuc}C_{elec}\beta)^2}{E_{HOMO} - E_{LUMO}}}_{\text{orbital}} \quad (14)$$

In this equation, Q_{nuc} and Q_{elec} are the total charges on interacting atoms of nucleophile and electrophile, ϵ is the local dielectric constant, R is the distance between atoms of nucleophile and electrophile, C_{nuc} is the coefficient of atomic orbital of nucleophile in HOMO, C_{elec} is the coefficient of atomic orbital of electrophile in LUMO, β is the overlap integral, E_{HOMO} is the energy of HOMO nucleophile and E_{LUMO} is the energy of LUMO electrophile. Thus, the charge on atom in a molecule (q) and its electron density (C) are essential requirements for the solution of Klopman Equation (14). In the present study the effective atomic charges calculated with usage of both Mulliken and natural bond orbital (NBO), and the atomic orbital coefficient of LUMO calculated using B3LYP method for the compounds 1a-h are shown in Table 3. The charges and the coefficient of each compound are confined to the two centers for the nucleophilic substitution reaction, namely ($C_1, C_{1'}$). Both the Mulliken and NBO charges show that the C_1 is slightly positive charged than the ipso carbon $C_{1'}$ and the charge does not change significantly with variation of the substituent especially within the Mulliken and NBO scheme. The general inspection of the coefficient on the two ipso carbon atoms C_1 and $C_{1'}$ in LUMO shows that its value is greater for $C_{1'}$ compared to C_1 for all ethers under investigation, Table 3.

Thus, $C_{1'}$ can be considered as the hard-electrophilic center while C_1 is the soft one. As a result, one can suggest that the region selectivity of the nucleophilic reaction depends on the nature of the attacking nucleophile: where hard nucleophile which has low lying HOMO and usually a negatively charged, making the energy gap between LUMO of the ether and the HOMO of the nucleophile is large, so the orbital term in Klopman equation would be very small and can be neglected, in such case the reaction is referred to as charge controlled and occur selectively on the carbon $C_{1'}$ and it will be kinetically fast due to a large electrostatic attraction. While for soft nucleophile which has high lying HOMO and not necessarily have a negative charge, make the HOMO of the nucleophile and the LUMO of the ether closer to each other which led to small denominator of the orbital term, consequently the orbital term has large value and so large influence of the orbital coefficients c and the resonance integral, in this case the reaction is referred to as FMO controlled and would occur selectively on C_1 . However, the interactions on each center can exhibit a mixture of charge and FMO contributions for nucleophiles of intermediate lying HOMO. The study of bond angles and lengths in the expected activated complexes II-1, II-2, III-1 and III-2 due to the attack of nitrogen and oxygen nucleophiles shed light on the mode of attack of N- and O-nucleophiles. Table 12 shows that bond angles $O_{11}-C_1-N_7$ and $O_{11}-C_{1'}-N_7$ in II-1 and II-2 are 95.7° and 94.9° points out that the mode of attack of aniline on C_1 or $C_{1'}$ is quit perpendicular. While, the central atom of $C_1-O_{11}-C_{1'}$ in both II intermediates still acquiring the sp^2 hybridization. Also, C_1-O_{11} and $C_{1'}-N$ bond length in II-1 are longer than those in II-2. On the other hand, all bond lengths involved in the nucleophilic attack are the same while mode of oxygen nucleophile attack is not quit perpendicular.

Synthesis of aryl 2,4-dinitro-1-naphthyl amine 2a-g: Aryl 2,4-dinitro-1-naphthyl amine compounds **2a-g** were prepared by substitution of the chlorine substituent of phenyl 1-(2,4-dinitronaphthyl) ether **1a** by 3- or 4-monosubstituted or 3,4-disubstituted aniline derivatives ($Y = H, OCH_3, CH_3, Cl$) **Equation (15)**. The chemical structures of the products **2a-g** are N-aryl 1-(2,4-dinitronaphthyl) amines, as proved from their elemental analysis, IR and 1H NMR spectra, as **Equation (15)**.(42). The main infrared absorption bands of compounds **2a-g** showed weak bands in the region $2947-3117\text{ cm}^{-1}$ correspond to the aromatic $sp^2=C-H$. While the NO_2 group exhibited two strong absorption bands for asymmetric and symmetric stretching at ranges $1528-1560$ and $1265-1316\text{ cm}^{-1}$, respectively.(16) Moreover, the medium to weak bands in the range $3246-3445\text{ cm}^{-1}$ is due to N-H stretching vibration bond (17). The low frequency values for N-H stretching in product can be attributed to hydrogen bonding between N-H and ortho-nitro group.

The 1H NMR spectra of amines **2a-g** showed a singlet signal of naphthalene H_3 in range $\delta 9.11 - 9.2$ ppm, while H_5 and H_8 appeared as two doublets in all compounds in range $\delta 7.98 - 8.69$ ppm. The signal for H_6 and H_7 of naphthalene ring appeared as two triplet signal (1 H each) in range $\delta 7.71 - 8.69$ ppm. The para phenyl H_2 and H_6 protons show doublet at range $\delta 6.96-7.12$ ppm, while H_3 and H_5 protons showed doublet signal (2H) in range $\delta 6.86-7.28$ ppm. The *meta* substituted 3-methyl **2d**, 3-chloro **2g** and 3-methoxy **2e** derivatives exhibited triplet for H_5 in ranges $\delta 7.19-7.22$ ppm. The unsubstituted H (**4d**) show triplet at $\delta 7.32$ for H_3 , H_4 and H_5 the methyl substituent in compounds 3-methoxy **2e**, 3-methyl **2d**, 4-methyl **2c** and 4-methoxy **2b** showed a singlet (3H) in range $\delta 2.23 - 3.8$ ppm

Optimized geometry of N-aryl 1-(2,4-dinitronaphthyl) amine 2a-g: The optimized molecular structure of amines **2a-g** are compared with phenyl 1-naphthyl amine (PNA) **5** which are calculated by B3LYP/ 6-311G(d,p) level. Such calculation uses these theoretical results to compare the molecular structure and nature of substituted amines **2b-g** against unsubstituted amine **2a** and phenyl 1-naphthyl amine **5**. The optimized geometrical parameters (bond length, angles and dihedral angles and atomic charges) of N-phenyl-1-naphthylamine **5** is listed in Tables 13 and 14 and shown in Figure 11. The calculated values in Table 6 show that bond lengths of C_1-N_{11} and $C_{1'}-N_{11}$ are slightly different. This is presumably due to the delocalization of the lone pair of electrons on N_{11}

with the phenyl ring is less pronounced than do with the naphthyl ring. While bond angles $N_{11}-C_1-C_2$ and $C_2-C_{11}-N_{11}$ as well as dihedral angles $C_2-C_1-N_{11}-C_{11}$ and $C_2-C_{11}-N_{11}-C_1$ indicate that the phenyl and naphthyl rings are not planar.

Molecular structure and optimized geometry of N-aryl 1-(2,4-dinitronaphthyl) amine 2a-g: The optimized molecular structure of N-aryl 1-(2,4-dinitronaphthyl) amines **2a-g** are calculated by B3LYP/6-311G (d, p) level and tabulated in Tables 15-17 and compared with the experimental data. No solvent corrections were made with these calculations. The computations were converged upon a true energy minimum, which were supported by the absence of imaginary frequencies. The chemical structures of compounds **2a-g** are shown in Figure 12.

Bond length: The influence of substituent groups in aryl moiety on C_1-N_{11} bond distances seem to be negligible while C_1-N_{11} bond lengths which are slightly different from the unsubstituted compound **2a**. Also, there is no observable effect on bonds cited in Table 15

Bond angles and Dihedral angles: Tables 16 and 17 show that there is no effect of substituent in the aryl moiety on bond angles and dihedral angles cited.

Mulliken charges: The Mulliken atomic charges of amines **2a-g** calculated at the B3LYP/6-311G (d, p) level in gas-phase are presented in Table 18. The Mulliken charge distribution shows that the charge of amine nitrogen atom N is not changed with the change in nature of substituents and negative (~ -0.465 to -0.471) as compared to positive charge of N in NO_2 groups ring N (~ 0.146) in all selected compounds. It has also been observed that most C atoms are positive and some are negative.

Molecular Electrostatic Potential (MEP): In MEP plots calculated for the amine products **2a-g** by B3LYP/6-311G (d, p) level are represented in Figure 13. The negative regions represented by red color, are preferable sites for electrophilic attack and the positive regions represented by blue color are favored toward nucleophilic attack. Here in all amines, the negative and less potentials regions are generated over the electronegative O atoms whereas the C-atoms in benzene and naphthalene rings and N-atoms have the positive and neutral potential regions in the structure. The negative and positive sites help to predict the regions in a compound responsible for non-covalent interactions (43).

Vibrational assignments of 2a-g: The computational study was extended to IR spectroscopy in order to support the assignment of experimental values of the vibration bands namely NH, sp^2 CH and NO_2 for **2a-g**. No imaginary frequencies were found thus eliminating saddle points in the potential hyper energy surface. The most characteristic band for each of the compounds is the N-H amine bond stretch found in the range of $3246-3445\text{ cm}^{-1}$ which is in congruent with the calculated range of amine vibrations in the $3419-3439\text{ cm}^{-1}$ range, Table 19. It indicates the formation of substituted amine. For aromatic compounds, the C-H stretching modes are experimentally observed in the region $3088-2915\text{ cm}^{-1}$. Figure 14 shows a great matching between experimental and calculating sheet of IR of compounds **2a-g**. The $\nu_{Ar} = C-H$ stretching modes are observed at $\sim 2915-3117\text{ cm}^{-1}$ in the IR spectrum for compounds **2a-g**, while the corresponding computed bands at $\sim 3165-3252\text{ cm}^{-1}$ in the IR spectrum are shown in Table 20. The asymmetric NO_2 stretching vibrations are generally observed in the region $1570-1485\text{ cm}^{-1}$, while the symmetric stretch appears between 1370 and 1320 cm^{-1} (44). It is interesting to mention that the most intense lines in the IR spectrum of appear at $3246-3445$, $1528-1560$ and $1269-1316\text{ cm}^{-1}$ are attributed to ν_{N-H} , ν_{NO_2} asym and ν_{NO_2} sym, respectively, corresponding computed bands are $3419-3439$, $1489-1586$ and $1309-1362\text{ cm}^{-1}$. Table 19.

UV-Visible analysis of 2a-g: Ultraviolet spectrum analysis of **2a-g** has been investigated by RTD-CAM-B3LYP/6-311G (d, p) method. The calculated visible absorption maxima of λ_{max} which is the function of the electron availability have been reported in Table 21. Molecular orbital geometry calculations show that the visible absorption maxima of this molecule correspond to the frontier orbitals electron transition between HOMO and LUMO. The calculated results involving the vertical excitation energies, oscillator strength f and wavelength are listed in Table 21. RTD-CAM-B3LYP/6-311G (d, p) method predict one intense electronic transition at $\lambda_{max} = 385-272\text{ nm}$ with an oscillator strength $f = 0.351-0.021$ which is in quit agreement with the measured experimental data $\lambda_{max} = 400-360\text{ nm}$ as shown in Figure 15.

Molecular orbital analysis of 2a-g: According to Koopmans theorem (45) global properties can be obtained by the Frontier Molecular Orbital (FMO) energies. In DFT, chemical potential (I_p) is defined as the amount of energy needed to remove an electron from a molecule. High ionization energy indicates high stability and chemical inertness while small ionization energy indicates high reactivity of the atoms and molecules. The electronic affinity (E_A) is defined as the energy released when an electron is added to a neutral molecule. A molecule with high (E_A) values tends to take electrons easily. The electronegativity (χ), describes the ability of a molecule to attract electrons towards itself in a covalent bond. Global hardness (η) and softness (S) are a useful concept for understanding the behavior of chemical systems. A hard molecule has a large energy gap and a soft molecule has a small energy gap. Therefore, soft molecules will be more polarizable than hard molecules. Global electrophilicity index (ω) is a combined descriptor involving chemical potential and hardness which expresses propensity of a species to accept electron. (46) The values of the calculated quantum chemical parameters like global hardness (η) global softness (S), electronegativity (χ), chemical potential (μ) and electrophilicity index (ω) are summarized in Table 22.

The energy of highest occupied molecular orbital (E_{HOMO}) and the lowest unoccupied molecular orbital (E_{LUMO}), energy gap ΔE_{gap} calculated by the B3LYP/6-311G (d, p) level in gas-phase are presented in Table 22. It reports the values of the electronic energies

calculated for all amine products 2a-g describe their reactivity. The optimized energy for these amines varies between (-1541.181, -1081.561 a.u). The Highest occupied molecular orbital (HOMO) and the lowest unoccupied molecular orbital (LUMO) plots of 2a-g molecule are presented in Figure 16 in the HOMO of all synthesized compounds; the electron density mainly delocalized over associate naphthalene ring and amino group. While in the LUMO orbital this density is delocalized over the entire molecule.

High ionization energy I_p indicates high stability and chemical inertness while small ionization energy E_A indicates high reactivity of the molecules. The values of I_p point out that amine 2b, (Y= 4-OCH₃) has the least ionization potential value (I_p = 6.17eV), and in turn it is the best electron donor and of lowest stability. While amine 3g, (Y= 3-Cl) has the highest ionization potential (I_p = 6.64 eV), highest stability and of poorest electron donor. However, the I_p values of compounds (2a-g) are of small difference between change in the nature and position of substituents. Also, the electronic affinity E_A values show the same behavior as I_p . i.e. both parameters are seen to be slightly depends on the nature of substituents in the aryl moiety. The dipole moment μ (D) is the most widely used quantity to describe the polarity of a covalent bond that results from non-uniform distribution of charges on the various atoms in the molecule. The order of polarity is arranged in the following order: 3b, (Y= 4-OCH₃) > 3e, (Y= 3-OCH₃) > 3c, (Y= 4-CH₃) > 3d, (Y= 3-CH₃) > 3a, (Y= H) > 3g, (Y= 3-Cl) > 3f, (Y= 4-Cl). The high value of dipole moment probably increases the reactivity of the molecule towards the reacting species

Table 22 shows that the chemical reactivity (χ eV) slightly varies with the structural of molecules. Chemical hardness (softness) value of compound 2b, (Y = 4-OCH₃) is lesser (greater) among all the molecules. Thus, compound 2b, (Y = 4-OCH₃) is found to be more reactive than all the molecules. Compound 2g, (Y = 3-Cl) possesses higher electronegativity value than all compounds so; it is the best electron acceptor. The values of (ω) for compounds 2a-g indicate that compounds contain electron withdrawing group have higher values of electrophilicity index which shows that the compounds of this group are a strong electrophiles than compounds contain electron donating substituents, Table 22.

Synthesis and assignments of 1-(2,4-dinitronaphthalen-1-yl) piperidine 3: The reaction between ether derivatives 1a-h and piperidine in DMSO yielded the expected 1-(2,4-dinitronaphthalen-1-yl) piperidine 3 and substituted phenol 4a-h with no side products detected independent on the nature of the aryl moiety, Equation (16). The structure of substitution product 3(47) indicated piperidination-dearyloxylation process.

Optimized geometry of 1-(2,4-dinitro naphthalen-1-yl) piperidine 3: We optimized 1-naphthyl piperidine 6 as a reference to compare with 1-(2,4-dinitro naphthalen-1-yl) piperidine 3 to determine the effect of introduction of 2- and 4-nitro substituents on the molecular structure parameters.

Optimized geometry of 1-naphthyl piperidine 6: The results of B3LYP/6-311G(d,p) calculations of the optimized geometrical parameters (bond length, angles and dihedral angles and atomic charges) and the numbering of atoms of 1-naphthyl piperidine 6 are listed in Tables 23 and 24 and shown in Figure 17.

The calculated values in Table 23 show that bond lengths of C₁-N₁ and C₁₁-N₁ are slightly different. This is presumably due to the delocalization of the lone pair of electrons on N₁ with the phenyl ring is less pronounced than do with the naphthyl ring. While bond angles C₂-N₁-C₁ and N₁-C₁-C₂ as well as dihedral angles C₂-N₁-C₁-C₂ and C₂-N₁-C₁-C₉ indicate that the phenyl and naphthyl rings are not planar. The Mulliken charge distribution shows that the charge of nitrogen atom N is not changed with the change in nature of substituents and negative -0.457 as compared to N in compound 3 N -0.479. It has also been observed that most C atoms are positive and some are negative that shown in Table 24

Theoretical Study of 1-(2,4-dinitro naphthalen-1-yl) piperidine 3: The optimized geometry of compound 3 was validated by frequency calculation which gave real values for all the obtained frequencies and no imaginary frequencies were found meaning that the structure has minimum potential energy. Among the chemical descriptors for which DFT/B3LYP provides good description include the energy of the highest occupied molecular orbital (E_{HOMO}), the energy of the lowest unoccupied molecular orbital (E_{LUMO}) and related properties such as hardness (η), softness (S), electronegativity (χ), electrophilicity (ω) and nucleophilicity indexes (Nu index). The optimized structural parameters determined at B3LYP level theory with 6-311G (d, p) basis set such as bond lengths, bond angle and dihedral angles of 3 are presented in Table 25 in accordance with the atom numbering scheme of the molecule shown in Figure 18. The bond lengths between carbon and nitrogen atoms in 3 are shorter than compound 6 and the remaining bonds may be due to the influence of the nitrogen atom on the molecular structure. Table 25 shows that all bond lengths of naphthalene ring and piperidiny moiety indicate double bond character.

Population Analysis: The Mulliken, NBO population analysis of 3 is computed using B3LYP with 6-311G (d, p) basis set and are listed in Table 26. The Mulliken charge of C₁ in naphthyl ring is more positive value than in 3 than 6. Other ring carbon atom having same values in the two molecules but only there is small variation in their magnitude. The charge of nitrogen atom N₁ is slightly high negative value for 3 compared to 6. The charges of hydrogen atoms connected to the ring of all three molecules are positive but there is slight variation in magnitude. The oxygen atoms O₁₂ and O₁₃ charge are negative magnitude is observed.

Vibrational assignments: The distribution of some modes of 3 which have been performed on the recorded IR theoretically predicted wave numbers are presented in Table 27. The calculated infrared wave numbers were well correlated with the intensities of the observed fundamental modes. The IR spectra from theoretical method are shown in Figure 19 the IR spectra from experimental shown in lit.(48). Aromatic nitro compounds have strong absorptions due to the asymmetric and symmetric

stretching vibrations of the NO₂ group at 1570–1485 and 1370–1320 cm⁻¹, respectively.(43)In the present molecule**3**, the band at 1622 and 1641 cm⁻¹by DFT method has been assigned to asymmetric stretching mode of NO₂ while the band at 1377 and 1361 cm⁻¹ has been assigned to symmetric stretching mode of NO₂ by DFT/B3LYP method. The bands corresponding to bending vibrations of NO₂ group were found well with the characteristic region and are summarized in Table 27.Also, the C–NO₂ stretching vibration is theoretically computed at 942, 1000 cm⁻¹.

Table 28 Shown the existence of one or more aromatic rings in a structure is normally readily determined from the C–H vibrations. The C–H stretching vibration occurs above 3000 cm⁻¹ and is typically exhibited as a multiplicity of weak to moderate bands, compared with the aliphatic C–H stretch. (49) In our present work, the C–H stretching vibration of ring is observed in FT-IR at 3098 cm⁻¹. The same vibration is calculated at 3081 and 3071 cm⁻¹ by B3LYP/6-311G (d, p) method. All the aromatic C–H stretching bands are found (49).

UV–Visible analysis: Ultraviolet spectra analysis of 1-(2,4-dinitronaphthalen-1-yl) piperidine **3** has been investigated in DMSO phase by theoretical calculation and are within 200–400 nm range. On the basis of fully optimized ground-state structure, TD-DFT/ CAM-B3LYP/6-311++G (d, p) calculations have been used to determine the low-lying excited states of **3**. The calculated visible absorption maxima of λ_{\max} which is a function of the electron availability have been reported in **Table 29**. The theoretical electronic excitation energies, oscillator strengths f , calculated by the TD-DFT method for the same solvent and are also listed in **Table 29**. Calculations of the molecular orbital geometry show that the visible absorption maxima of this molecule correspond to the electron transition between frontier orbitals such as transition from HOMO → LUMO. As can be seen from **Table 29**, the calculated absorption maxima values have been found to be 449-288 nm for DMSO solution at DFT/CAM-B3LYP/6-311++G (d,p), DFT/CAM-B3LYP/6-311G (d,p) and DFT/B3LYP/6-311G (d,p) methods. As can be seen from **Figure 20**, **Table 29** calculations performed at DMSO phase.

NMR Spectra Analysis

The full geometry optimization of 1-(2,4-dinitronaphthalen-1-yl) piperidine**3** was performed by using B3LYP/6-311G(d,p), BLYP/6-311G(d,p) methods and GIAO ¹H chemical shift calculations in CDCl₃ of the of the **3**have been made by same methods, **Table30**.

Molecular orbital analysis:

The energy gap for **3** was calculated using B3LYP/6-311G (d, p) level. LUMO as an electron acceptor represents the ability to obtain an electron; donor represents the ability to donate an electron. The frontier molecular orbital of **3** (HOMO–LUMO) is shown in **Table 31**, **Figure 22**. HOMO energy= -6.40 eV,LUMO energy= -3.04 eV,Energy gap= 3.36 eV. I_p = Ionization potential (eV), E_A = electron affinity (eV). The ionizationpotential and electron affinity of the title molecule in gas phase is calculated at 6.40 eV and 3.04 eV respectively. Considering the global hardness, softness and electrophilicity index (50) are 1.68, 0.06 and 6.64 respectively. Large and small energy gap indicates the hard/soft molecules respectively. One can also relate the stability of molecule to hardness, which means that the molecule with least energy gap, it can be more reactive.

Molecular Electrostatic Potential (MEP)

MEP studies was carried out by B3LYP using 6-311G (d, p) basis set, **Figure 23**. Potential increases in the order red < orange < yellow < green < blue. Where blue denoting extremely electron deficient regions and red denoting electron rich regions. As can be seen from the **Figure 23**, also in support with the literature(51).

EXPERIMENTAL

The IR spectra were recorded for potassium bromide (KBr) discs on a Perkin-Elmer FT-IR, System spectrum ratio recording infra-red spectrophotometer, Faculty of Science, Alexandria University. The IR spectra were recorded for potassium bromide (KBr) discs on FTR-84005 Fourier transform Shimadzu, System spectrum ratio recording infra-red spectrophotometer, Central Laboratory Unit, Universities and Research centres District new Borg El-Arab City. The NMR spectra were carried out at ambient temperature (~25 °C) on a (JEOL) 500 MHz spectrophotometer using tetra methyl silane (TMS) as an internal standard, Central Laboratory Unit, Faculty of Science, Alexandria University.

Method of Calculations

All computational calculations have been performed on personal computer using the Gaussian 09W program packages developed by Frisch and coworkers(52). The Becke's three parameter hybrid functional using the LYP correlation functional (B3LYP), one of the most robust functional of the hybrid family, was herein used for all the calculations, with 6.311G (d, p) basis set. (53)

Preparation of Aryl 1-(2,4-dinitro-1-naphthyl) ether 1a-h:

1-Chloro-2,4-dinitronaphthalene (1 g, 3.96 mmol) was dissolved in 20 mL chloroform. The ethereal solution of sodium substituted phenoxide (4 mmol) was added dropwise to the reaction mixture at room temperature. The reaction mixture was stirred for 30-90 min then the formed precipitate was filtered, dried and crystalized from appropriate solvent.

Phenyl 1-(2,4-dinitronaphthyl) ether 1a:

Yellow needles 0.61 g (95%) yield; m.p. 181-182 °C. IR (KBr): 3084 (sp²= C-H), 1539, 1359 (NO₂ asymmetric and symmetric stretching) and 1209 1041 (C-O, asymmetric and symmetric stretching) cm⁻¹. ¹H-NMR (500 MHz: DMSO),: δ 3.76 (s, 3H, -OCH₃), 6.96 (d, 2H, J = 8.4 Hz, H₂' and H₆'), 7.10 (t, 1H, H₄'), 7.32 (t, 2H, H₃' and H₅'), 7.84 (t, 1H, J = 7.65 Hz, H₇'), 8.03 (t, 1H, H₆'), 8.21 (d, 1H, J = 8.4 Hz, H₈'), 8.52 (d, 1H, J = 9.15 Hz, H₅'), 8.94 (s, 1H, H₃) ppm.

4-Anisyl 1-(2,4-dinitronaphthyl ether) 1b:

Yellow needles 0.61 g (91%) yield; m.p. 152 °C. IR (KBr): 3085 ($\text{sp}^2=\text{C-H}$), 1532, 1339 (NO_2 , asymmetric and symmetric stretching) and 1231, 1025 (C-O, asymmetric and symmetric stretching) cm^{-1} . $^1\text{H-NMR}$ (500 MHz: CDCl_3): δ 3.76(s, 3H, 4-OCH₃), 6.79-6.81 (m, 4H, Ar-H), 7.75 (t, 1H, H₇), 7.92 (t, 1H, H₆), 8.40 (d, 1H, H₈), 8.71 (d, 1H, $J=8.4$ Hz, H₅), 8.84 (s, 1H, H₃) ppm. Mass spectra, show molecular ion peak at $m/z = 340$.

4-Tolyl 1-(2,4-dinitronaphthyl) ether 1c:

Yellow needles 0.6 g (93%) yield; m.p. 158-159 °C. IR (KBr): 3068 ($\text{sp}^2=\text{C-H}$), 1541, 1359 (NO_2 , asymmetric and symmetric stretching) and 1207, 962 (C-O, asymmetric and symmetric stretching) cm^{-1} . $^1\text{H-NMR}$ (500 MHz: CDCl_3): δ 2.30 (s, 3H, 4-CH₃), 6.75 (d, 2H, $J=9.2$ Hz, H_{2'} and H_{6'}), 7.09 (d, 2H, $J=8.4$ Hz, H_{3'} and H_{5'}), 7.74 (t, 1H, H₇), 7.94 (t, 1H, H₆), 8.38 (d, 1H, $J=8.4$ Hz, H₈), 8.72 (d, 1H, $J=9.2$ Hz, H₅), 8.86 (s, 1H, H₃) ppm. Mass spectra, show molecular ion peak at $m/z = 324$.

3-Tolyl 1-(2,4-dinitronaphthyl) ether 1d:

Yellow needles 0.62 g (94%) yield; m.p. 113-115 °C.; 3086 ($\text{sp}^2=\text{C-H}$), 1530, 1339 (NO_2 , asymmetric and symmetric stretching) and 1241, 1085 (C-O, asymmetric and symmetric stretching) cm^{-1} . $^1\text{H-NMR}$ (500 MHz: CDCl_3): δ 2.30 (s, 3H, 3-CH₃), 6.63 (d, 2H, H_{6'}), 6.69 (s, 1H, H_{2'}), 6.92 (d, 1H, $J=7.65$ Hz, H_{4'}), 7.17 (t, 1H, H_{5'}), 7.74 (t, 1H, H₇), 7.93 (t, 1H, H₆), 8.36 (d, 1H, H₈), 8.72 (d, 1H, $J=8.4$ Hz, H₅), 8.88 (s, 1H, H₃) ppm. Mass spectra, show molecular ion peak at $m/z = 324$.

3-Anisyl 1-(2,4-dinitronaphthyl) ether 1e:

Pale yellow crystals 0.59 g (88%) yield; m.p. 130-132 °C. IR (KBr): 3075 ($\text{sp}^2=\text{C-H}$), 1530, 1347 (NO_2 , asymmetric and symmetric stretching) and 1268, 1035 (C-O, asymmetric and symmetric stretching) cm^{-1} . $^1\text{H-NMR}$ (500 MHz: CDCl_3): δ 3.78 (s, 3H, 3-OCH₃), 6.35 (d, 1H, H_{6'}), 6.49 (s, 1H, H_{2'}), 6.66 (d, 1H, H_{4'}), 7.18 (t, 1H, H_{5'}), 7.74 (t, 1H, H₇), 7.94 (t, 1H, H₆), 8.35 (d, 1H, $J=8.4$ Hz, H₈), 8.71 (d, 1H, $J=8.45$ Hz, H₅), 8.88 (s, 1H, H₃) ppm. Mass spectra, show molecular ion peak at $m/z = 340$.

4-Chlorophenyl 1-(2,4-dinitronaphthyl) ether 1f:

Yellow needles 0.66 g (95%) yield; m.p. 164 °C.; 3078 ($\text{sp}^2=\text{C-H}$), 1535, 1346 (NO_2 , asymmetric and symmetric stretching) and 1116-950 (C-O, asymmetric and symmetric stretching) cm^{-1} . $^1\text{H-NMR}$ (500 MHz: CDCl_3): δ 6.80 (d, 2H, $J=9.2$ Hz, H_{2'} and H_{6'}), 7.32 (d, 2H, $J=8.4$ Hz, H_{3'} and H_{5'}), 7.76 (t, 1H, H₇), 7.96 (t, 1H, H₆), 8.31 (d, 1H, $J=9.15$ Hz, H₈), 8.72 (d, 1H, $J=8.4$ Hz, H₅), 8.87 (s, 1H, H₃) ppm. Mass spectra, show molecular ion peak at $m/z = 344$.

3-Chlorophenyl 1-(2,4-dinitronaphthyl) ether 1g:

Yellow needles 0.66 g (95%) yield; m.p. 115-117 °C. IR (KBr): 3084 ($\text{sp}^2=\text{C-H}$), 1528, 1341 (NO_2 , asymmetric and symmetric stretching) and 1268-1085 (C-O, asymmetric and symmetric stretching) cm^{-1} . $^1\text{H-NMR}$ (500 MHz: CDCl_3): δ 6.75 (d, 1H, $J=8.4$ Hz, H_{6'}), 6.88 (s, 1H, H_{2'}), 7.11 (d, 1H, $J=7.6$ Hz, H_{4'}), 7.24 (t, 1H, H_{5'}), 7.77 (t, 1H, H₇), 7.95 (t, 1H, H₆), 8.30 (d, 1H, $J=8.4$ Hz, H₈), 8.72 (d, 1H, $J=9.1$ Hz, H₅), 8.69 (s, 1H, H₃) ppm. Mass spectra, show molecular ion peak at $m/z = 344$.

4-Nitrophenyl 1-(2,4-dinitronaphthyl) ether 1h:

Pale yellow crystals 0.61 g (91%) yield; m.p. 132 °C; IR (KBr): 3087 ($\text{sp}^2=\text{C-H}$), 1528, 1344 (NO_2 , asymmetric and symmetric stretching) and 1232, 1107 (C-O, asymmetric and symmetric stretching) cm^{-1} . $^1\text{H-NMR}$ (500 MHz: CDCl_3): δ 6.68 (d, 2H, $J=9.2$ Hz, H_{2'} and H_{6'}), 8.23 (d, 2H, $J=9.15$ Hz, H_{3'} and H_{5'}), 8.90 (s, 1H, H₃), 7.99 (t, 1H, $J=7.65$ Hz, H₆), 7.80 (t, 1H, H₇), 8.22 (d, 1H, H₈), 8.72 (d, 1H, $J=6.8$ Hz, H₅) ppm. Mass spectra, show molecular ion peak at $m/z = 355$.

Preparation of 2,4-dinitro-1-naphthyl substituted phenyl amine 2a-g:

Phenyl 1-(2,4-dinitronaphthyl) ether **1a** (1 g, 3.23 mmol) was dissolved in 20 ml DMSO and then substituted aniline dissolved in 20ml DMSO was added drop wise to it at room temperature. The reaction mixture was stirred and refluxed for 7 hours, the formed precipitate was filtered, dried, and crystalized from ethyl acetate/ petroleum ether. The purity was checked by TLC (8:2 petroleum ether: ethyl acetate).

2,4-dinitro-N-phenylnaphthalene-1-amine 2a:

Orange crystals, Yield: 92% after 8 hours, m.p. 185 °C. IR (KBr), 3300 (NH), 3088 ($\text{sp}^2=\text{C-H}$), 1537, 1290 (NO_2 , asymmetric and symmetric stretching) cm^{-1} . $^1\text{H-NMR}$ (500 MHz: CDCl_3), δ 7.04 (d, 2H, $J=8.4$ Hz, H_{2'} and H_{6'}), 7.2 (t, 1H, $J=7.65$ Hz, H₇), 7.32 (t, 3H, $J=8.4$ Hz, H_{3'}, H_{4'} and H_{5'}), 7.75 (t, 1H, $J=7.65$ Hz, H₆), 8.01 (d, 1H, $J=8.4$ Hz, H₈), 8.68 (d, 1H, $J=8.4$ Hz, H₅), 9.15 (s, 1H, H₃), 10.61 (s, 1H, NH, D₂O exchangeable). C₁₆H₁₁N₃O₄: Calc. C, 62.14; H, 3.58; N, 13.59; O, 20.69%. Found: C, 62.48; H, 3.19; N, 13.73; O, 20.31 %.

N-(4-methoxyphenyl)-2,4-dinitronaphthalene-1-amine 2b:

Crimson red crystals, Yield: 89% after 6 hours, m.p. 205-207 °C. IR (KBr), 3439 (NH), 2955 ($\text{sp}^2=\text{C-H}$), 1545, 1269 (NO_2 , asymmetric and symmetric stretching) cm^{-1} . $^1\text{H-NMR}$ (500 MHz: CDCl_3), δ 3.8 (s, 3H, H₄), 6.86 (d, 2H, $J=8.4$ Hz, H_{2'} and H_{6'}), 7.02 (d, 2H, $J=9.15$ Hz, H_{3'} and H_{5'}), 7.3 (t, 1H, $J=6.9$ Hz, H₇), 7.71 (t, 1H, $J=7.65$ Hz, H₆), 8.0 (d, 1H, $J=9.15$ Hz, H₈), 8.67 (d, 1H, $J=8.4$ Hz, H₅), 9.17 (s, 1H, H₃), 10.82 (s, 1H, NH, D₂O exchangeable). C₁₇H₁₃N₃O₅: Calc. C, 60.18; H, 3.86; N, 12.38; O, 23.58%. Found: C, 60.52; H, 3.51; N, 12.02; O, 23.24 %.

2,4-dinitro-N-(p-tolyl) naphthalene-1-amine 2c:

Orange crystals, Yield: 90% after 7 hours, m.p. 200 °C. IR (KBr): 3252 (NH), 3111 ($\text{sp}^2=\text{C-H}$), 1560, 1290 (NO_2 , asymmetric and symmetric stretching) cm^{-1} . $^1\text{H-NMR}$ (500 MHz: CDCl_3): δ 2.35 (s, 3H, H₄), 6.94 (d, 2H, $J=8.4$ Hz, H_{3'} and H_{5'}), 7.12 (d, 2H, $J=8.4$ Hz, H_{2'} and H_{6'}), 7.31 (t, 1H, $J=8.4$ Hz, H₇), 7.73 (t, 1H, $J=8.4$ Hz, H₆), 8.01 (d, 1H, $J=8.4$ Hz, H₈), 8.67 (d, 1H, $J=8.4$ Hz, H₅), 9.15 (s, 1H, H₃), 10.7 (s, 1H, NH, D₂O exchangeable). C₁₇H₁₃N₃O₄: Calc. C, 63.16; H, 4.05; N, 13; O, 19.79%. Found: C, 63.47; H, 4.36; N, 12.87; O, 19.38 %.

2,4-dinitro-N-(m-tolyl) naphthalene-1-amine 2d:

Orange crystals, Yield: 70% after 7 hours, m.p. 170 °C. IR (KBr), 3445 (NH), 2915 ($\text{sp}^2=\text{C-H}$), 1528, 1314 (NO_2 , asymmetric and symmetric stretching) cm^{-1} . $^1\text{H-NMR}$ (500 MHz: CDCl_3), δ 6.81 (d, 1H, $J=7.65$ Hz, H_{4'}), 6.9 (s, 1H, H_{2'}), 7.02 (d, 1H, $J=6.9$ Hz, H_{6'}), 7.19 (t, 1H, $J=7.65$ Hz, H_{5'}), 7.32 (t, 1H, $J=7.65$ Hz, H₇), 7.75 (t, 1H, $J=7.65$ Hz, H₆), 8.03 (d, 1H, $J=9.2$ Hz, H₈), 8.69 (d, 1H, $J=8.45$ Hz, H₅), 9.2 (s, 1H, H₃), 10.6 (s, 1H, NH, D₂O exchangeable). C₁₇H₁₃N₃O₄: Calc. C, 63.16; H, 4.05; N, 13; O, 19.79%. Found: C, 63.41; H, 3.98; N, 13.39; O, 20.12 %.

N-(3-methoxyphenyl)-2,4-dinitronaphthalene-1-amine 2e:

Red crystals, Yield: 88% after 9 hours, m.p. 184 °C. IR (KBr), 3296 (NH), 3075 ($\text{sp}^2=\text{C-H}$), 1545, 1308 (NO_2 , asymmetric and symmetric stretching) cm^{-1} . $^1\text{H-NMR}$ (500 MHz: CDCl_3), δ 3.74 (s, 3H, CH_3), 6.58 (d, 1H, $J = 7.65$ Hz, H_6'), 6.74 (d, 1H, $J = 8.4$ Hz, H_4'), 7.2 (t, 1H, $J = 8.4$ Hz, H_5'), 7.26 (s, 1H, H_2'), 7.35 (t, 1H, $J = 7.65$ Hz, H_7'), 7.75 (t, 1H, $J = 7.65$ Hz, H_6), 8.05 (d, 1H, $J = 8.4$ Hz, H_8), 8.68 (d, 1H, $J = 8.45$ Hz, H_3), 9.14 (s, 1H, H_3), 10.54 (s, 1H, NH, D_2O exchangeable). $\text{C}_{17}\text{H}_{13}\text{N}_3\text{O}_5$: Calc. C, 60.18; H, 3.86; N, 12.38; O, 23.58%. Found: C, 60.01; H, 3.49; N, 12.76; O, 23.18 %.

***N*-(4-chlorophenyl)-2,4-dinitronaphthalene-1-amine 2f:**

Golden yellow crystals, Yield: 89% after 10 hours, m.p. 208-210 °C. IR (KBr), 3246 (NH), 3117 ($\text{sp}^2=\text{C-H}$), 1543, 1277 (NO_2 , asymmetric and symmetric stretching) cm^{-1} . $^1\text{H-NMR}$ (500 MHz: CDCl_3), δ 6.96 (d, 2H, $J = 8.4$ Hz, H_2, H_6'), 7.28 (d, 2H, $J = 9.2$ Hz, H_3' and H_5'), 7.39 (t, 1H, $J = 7.65$ Hz, H_7'), 7.78 (t, 1H, $J = 8.4$ Hz, H_6), 7.98 (d, 1H, $J = 9.15$ Hz, H_8), 8.68 (d, 1H, $J = 8.4$ Hz, H_5), 9.13 (s, 1H, H_3), 10.45 (s, 1H, NH, D_2O exchangeable). $\text{C}_{16}\text{H}_{10}\text{ClN}_3\text{O}_4$: Calc. C, 55.91; H, 2.93; N, 12.33; O, 18.62; Cl, 10.31 %. Found: C, 56.28; H, 3.11; N, 12.56; O, 18.93; Cl, 10.65 %.

***N*-(3-chlorophenyl)-2,4-dinitronaphthalene-1-amine 2g:**

Orange crystals, Yield: 87% after 12 hours, m.p. 180 °C. IR (KBr), 3281 (NH), 3082 ($\text{sp}^2=\text{C-H}$), 1539, 1316 (NO_2 , asymmetric and symmetric stretching) cm^{-1} . $^1\text{H-NMR}$ (500 MHz: CDCl_3), δ 6.85 (d, 1H, $J = 8.4$ Hz, H_6'), 7.03 (s, 1H, H_2'), 7.15 (d, 1H, $J = 7.65$ Hz, H_4'), 7.22 (t, 1H, $J = 8.4$ Hz, H_5'), 7.42 (d, 1H, $J = 7.65$ Hz, H_7'), 7.8 (d, 1H, $J = 7.65$ Hz, H_6), 8.00 (d, 1H, $J = 8.4$ Hz, H_8), 8.69 (d, 1H, $J = 8.4$ Hz, H_5), 9.11 (s, 1H, H_3), 10.33 (s, 1H, NH, D_2O exchangeable). $\text{C}_{16}\text{H}_{10}\text{ClN}_3\text{O}_4$: Calc. C, 55.91; H, 2.93; N, 12.33; O, 18.62; Cl, 10.31 %. Found: C, 55.48; H, 3.32; N, 12.01; O, 18.27; Cl, 10.03 %.

REFERENCES

1. M. Fazal Mohamed, S. Arunadevi, M. Koperuncholan, M.S. Mubarak, *De r Chemica Sinica* 2 (2011) 52.
2. U. Rastuti, D. Siswanta, *Oriental Journal of Chemistry* 32 (2016) 2451.
3. A.M. El-Metwally, *EGYPTIAN JOURNAL OF CHEMISTRY* 54 (2011) 129.
4. C. Ibis, A.F. Tuyun, H. Bahar, S.S. Ayla, M.V. Stasevych, R.Y. Musyanovych, O. Komarovska-Porokhnyavets, V. Novikov, *Medicinal Chemistry Research* 23 (2014) 2140.
5. Y. Wang, P.-D. Mao, W.-N. Wu, X.-J. Mao, X.-L. Zhao, Z.-Q. Xu, Y.-C. Fan, Z.-H. Xu, *Sensors and Actuators B: Chemical* 251 (2017) 813.
6. V. Krishnakumar, N. Prabavathi, S. Muthunatesan, *Spectrochimica Acta Part A: Molecular and Biomolecular Spectroscopy* 69 (2008) 528.
7. H.R. Nasiri, M.G. Madej, R. Panisch, M. Lafontaine, J.W. Bats, C.R.D. Lancaster, H. Schwalbe, *Journal of medicinal chemistry* 56 (2013) 9530.
8. G.W. Winston, R.T. Di Giulio, *Aquatic toxicology* 19 (1991) 137.
9. T. Wolff, *Journal of environmental Sciences (China)* Vol 4 (1992) 74.
10. H.-W. Wang, D. Wang, R.-W. Dzung, *Cancer research* 44 (1984) 3098.
11. R. Altenburger, W. Brack, W.R. Greco, M. Grote, K. Jung, A. Ovari, J. Riedl, K. Schwab, E. Küster, *Environmental science & technology* 40 (2006) 6163.
12. S. Bertini, V. Calderone, I. Carboni, R. Maffei, A. Martelli, A. Martinelli, F. Minutolo, M. Rajabi, L. Testai, T. Tuccinardi, *Bioorganic & medicinal chemistry* 18 (2010) 6715.
13. H.-J. Cristau, P.P. Cellier, S. Hamada, J.-F. Spindler, M. Taillefer, *Organic letters* 6 (2004) 913.
14. E. Glendening, A. Reed, J. Carpenter, F. Weinhold, Inc.: Pittsburgh, PA (2003).
15. T. Ogawa, M. Sumita, Y. Shimodo, K. Morihashi, *Chemical Physics Letters* 511 (2011) 219.
16. Z. Daszkiewicz, J. Kyzioł, W. Preźdo, J. Zaleski, *Journal of Molecular Structure* 553 (2000) 9.
17. G. Socrates, *Journal of the American Chemical Society* 117 (1995) 1671.
18. M. Kandasamy, G. Velraj, S. Kalaichelvan, G. Mariappan, *Spectrochimica Acta Part A: Molecular and Biomolecular Spectroscopy* 134 (2015) 191.
19. W.J. Feast, M. Gimeno, A.M. Kenwright, *Macromolecules* 39 (2006) 4076.
20. K. Druzbicki, E. Mikuli, M.D. Ossowska-Chruściel, *Vibrational Spectroscopy* 52 (2010) 54.
21. D. Dołęga, A. Migdał-Mikuli, J. Chruściel, *Journal of Molecular Structure* 933 (2009) 30.
22. M. Snehalatha, C. Ravikumar, I.H. Joe, V. Jayakumar, *Journal of Raman Spectroscopy: An International Journal for Original Work in all Aspects of Raman Spectroscopy, Including Higher Order Processes, and also Brillouin and Rayleigh Scattering* 40 (2009) 1121.
23. P. Nagabalasubramanian, S. Periandy, S. Mohan, M. Govindarajan, *Spectrochimica Acta Part A: Molecular and Biomolecular Spectroscopy* 73 (2009) 277.
24. N. Obi-Egbedi, I. Obot, M.I. El-Khaiary, *Journal of Molecular Structure* 1002 (2011) 86.
25. G. Shakila, H. Saleem, N. Sundaraganesan, *World Scientific News* 61 (2017) 150.
26. P. Elliott, K. Burke, M.H. Cohen, A. Wasserman, *Physical Review A* 82 (2010) 024501.
27. J. Padmanabhan, R. Parthasarathi, V. Subramanian, P. Chattaraj, *The Journal of Physical Chemistry A* 111 (2007) 1358.
28. P.K. Chattaraj, S. Giri, *The Journal of Physical Chemistry A* 111 (2007) 11116.
29. R.G. Parr, L.v. Szentpály, S. Liu, *Journal of the American Chemical Society* 121 (1999) 1922.
30. L.A. Flippin, D.W. Gallagher, K. Jalali-Araghi, *The Journal of Organic Chemistry* 54 (1989) 1430.
31. K. Burke, L.O. Wagner, *International Journal of Quantum Chemistry* 113 (2013) 96.
32. D.M.A. Vera, A.B. Pierini, *Physical Chemistry Chemical Physics* 6 (2004) 2899.
33. A.F. Oliveira, G. Seifert, T. Heine, H.A. Duarte, *Journal of the Brazilian Chemical Society* 20 (2009) 1193.
34. N. Okulik, A. Jubert, *J. Mol. Des* 4 (2005) 5.27.
35. M.V. Putz, N. Russo, E. Sicilia, *Theoretical Chemistry Accounts* 114 (2005) 38.

36. A. Ünal, B. Eren, *Spectrochimica Acta Part A: Molecular and Biomolecular Spectroscopy* 114 (2013) 129.
37. N.M. Hamada, *ChemistryOpen* 7 (2018) 814.
38. K.I. Al-Malah, *Journal of molecular modeling* 17 (2011) 325.
39. M.F. Ibrahim, S. Senior, M.A. El-Atawy, S.K. El-Sadany, E.A. Hamed, *Journal of Molecular Structure* 1006 (2011) 303.
40. Y. Sharma, S. Chand and Co. ltd (2009).
41. G. Klopman, *Journal of the American Chemical Society* 90 (1968) 223.
42. P. Singh, F. Pasha, H. Srivastava, *QSAR & Combinatorial Science* 22 (2003) 843.
43. S.Y. Ebrahimipour, M. Abaszadeh, J. Castro, M. Seifi, *Polyhedron* 79 (2014) 138.
44. K.M. Al-Ahmary, R.A. Mekheimer, M.S. Al-Enezi, N.M. Hamada, M.M. Habeeb, *Journal of Molecular Liquids* 249 (2018) 501.
45. T. Koopmans, *Physica* 1 (1933) 104.
46. P.K. Chattaraj, U. Sarkar, D.R. Roy, *Chemical reviews* 106 (2006) 2065.
47. F. Jensen, *Introduction to computational chemistry*, John wiley & sons, 2017.
48. S. Sekiguchi, R. Hikage, K. Obana, K. Matsui, Y. Ando, N. Tomoto, *Bulletin of the Chemical Society of Japan* 53 (1980) 2921.
49. J. Coates, *Encyclopedia of analytical chemistry: applications, theory and instrumentation* (2006).
50. T. Koopmans, *Physica* 1 (1934) 104.
51. Y. Bathini, I. Sidhu, R. Singh, R.G. Micetich, P.L. Toogood, *Tetrahedron letters* 43 (2002) 3295.
52. M. Frisch, G. Trucks, H. Schlegel, G. Scuseria, M. Robb, J. Cheeseman, G. Scalmani, V. Barone, B. Mennucci, G. Petersson, Wallingford, CT (2008).
53. H.B. Schlegel, *Journal of Computational Chemistry* 3 (1982) 214.
